CellPress

Molecular Cell
Resource

Multiplexed and Programmable Regulation of Gene Networks with an Integrated RNA and CRISPR/Cas Toolkit in Human Cells

Lior Nissim,[1,2] Samuel D. Perli,[1,2] Alexandra Fridkin,[1] Pablo Perez-Pinera,[1] and Timothy K. Lu[1,*]
[1]Synthetic Biology Group, Research Laboratory of Electronics, Department of Biological Engineering and Electrical Engineering & Computer Science, Massachusetts Institute of Technology, Cambridge, MA 02142, USA
[2]Co-first authors
*Correspondence: timlu@mit.edu
http://dx.doi.org/10.1016/j.molcel.2014.04.022

SUMMARY

RNA-based regulation and CRISPR/Cas transcription factors (CRISPR-TFs) have the potential to be integrated for the tunable modulation of gene networks. A major limitation of this methodology is that guide RNAs (gRNAs) for CRISPR-TFs can only be expressed from RNA polymerase III promoters in human cells, limiting their use for conditional gene regulation. We present new strategies that enable expression of functional gRNAs from RNA polymerase II promoters and multiplexed production of proteins and gRNAs from a single transcript in human cells. We use multiple RNA regulatory strategies, including RNA-triple-helix structures, introns, microRNAs, and ribozymes, with Cas9-based CRISPR-TFs and Cas6/Csy4-based RNA processing. Using these tools, we efficiently modulate endogenous promoters and implement tunable synthetic circuits, including multistage cascades and RNA-dependent networks that can be rewired with Csy4 to achieve complex behaviors. This toolkit can be used for programming scalable gene circuits and perturbing endogenous networks for biology, therapeutic, and synthetic biology applications.

INTRODUCTION

The ability to build complex, robust, and scalable synthetic gene networks that operate with defined interconnections between artificial parts and native cellular processes is central to engineering biological systems (Cheng and Lu, 2012). This capability can also be used to rewire, perturb, and probe natural biological networks for basic biology and therapeutic purposes. A large set of tunable, orthogonal, compact, and multiplexable gene regulatory mechanisms is of fundamental importance for these applications. However, the tools that are currently available fail to meet one or more of the criteria described above. For example, transcriptional regulation utilizes transcription factors that bind predetermined DNA sequences of interest. Previously, natural DNA-binding proteins have been used to target effector domains, such as activators and repressors, to the regulatory regions of mammalian genes to modulate their transcription (Cronin et al., 2001; Gossen and Bujard, 1992). However, only a few orthogonal variants of natural DNA-binding proteins are well characterized, and modifying their sequence specificity is challenging (Urlinger et al., 2000). Other approaches have focused on engineering artificial DNA-binding proteins such as zinc fingers and transcription-activator-like effectors, which can require multistep assembly, screening, and/or optimization processes to achieve desired DNA binding characteristics (Beerli and Barbas, 2002; Blount et al., 2012; Khalil et al., 2012; Purcell et al., 2013; Reyon et al., 2012).

Recently, type II CRISPR/Cas systems (DNA-targeting Cas proteins) have been adapted to achieve programmable DNA binding without requiring complex protein engineering (Sander and Joung, 2014). In these systems, the sequence specificity of the Cas9 DNA-binding protein is determined by guide RNAs (gRNAs) that have base-pairing complementarity to DNA target sites. This enables simple and highly flexible programing of Cas9 binding. Cas9's nuclease activity has been adapted for precise and efficient genome editing in prokaryotic and eukaryotic cells (Cong et al., 2013; Jiang et al., 2013; Jinek et al., 2012, 2013; Mali et al., 2013b). A mutant derivative of this protein (dCas9), which lacks nuclease activity, was modified to enable programmable transcriptional regulation of both ectopic and native promoters to create CRISPR-based transcription factors (CRISPR-TFs) in mammalian cells (Cheng et al., 2013; Farzadfard et al., 2013; Gilbert et al., 2013; Maeder et al., 2013; Mali et al., 2013a; Perez-Pinera et al., 2013). Type III CRISPR/Cas systems (RNA-targeting Cas proteins) have also been adapted for synthetic biology applications (Qi et al., 2012). For example, the type III CRISPR/Cas-associated Csy4 protein from *Pseudomonas aeruginosa* has been used in bacteria to achieve predictable regulation of multigene operons by cleaving precursor mRNAs. The functionality of Csy4 has also been demonstrated in bacteria, archaea, and eukaryotes (Qi et al., 2012).

CRISPR-TFs can enable the construction of large-scale synthetic gene circuits and the rewiring of natural regulatory networks. This is due to the ease of defining new, orthogonal transcriptional regulators by designing artificial gRNAs. However, up until now, gRNAs in human cells have only been expressed from RNA polymerase III (RNAP III) promoters,

presumably since RNAs expressed from most RNA polymerase II (RNAP II) promoters are expected to be exported to the cytoplasm, while gRNAs and Cas9 need to interact with DNA in the nucleus. Because RNAP III promoters comprise only a small portion of cellular promoters and are mostly constitutively active (Orioli et al., 2012), this is an important limitation for programming CRISPR/Cas activity for conditional gene regulation and genome engineering. For example, conditional regulatory systems in which gRNA production is linked to tissue-specific (Chen et al., 2006), temporally controllable (Gauthier et al., 2010), and/or inducible expression systems (Karlsson et al., 2012) cannot be readily constructed with RNAP III promoters, whereas many such systems that utilize RNAP II promoters exist. Another limitation of existing CRISPR/Cas regulatory schemes is that multiple gRNAs are typically needed to efficiently activate endogenous promoters (Cheng et al., 2013; Maeder et al., 2013; Mali et al., 2013a; Perez-Pinera et al., 2013), but strategies for multiplexed gRNA production from single transcripts have not yet been described. As a result, multiple gRNA expression constructs are currently needed to perturb natural transcriptional networks, thus limiting scalability.

In addition to transcriptional regulation, natural circuits leverage RNA-based posttranscriptional regulation to achieve complex behaviors (Audibert et al., 2002; Chen and Manley, 2009; Lin et al., 2007; Mercer et al., 2009; Wilson and Doudna, 2013). Short hairpin RNAs (shRNAs) and microRNAs (miRNAs) have been expressed from both RNAP II and RNAP III promoters and can be embedded in 3′ UTRs or as introns (Greber et al., 2008; Shin et al., 2006; Stewart et al., 2003). Moreover, multiple miRNAs can be expressed concomitantly from the same transcript (Shin et al., 2006), and synthetic circuits that use shRNA- and miRNA-based regulation in mammalian systems have been built (Greber et al., 2008; Xie et al., 2011). Thus, gene regulatory strategies based on combining RNA engineering with transcriptional and posttranscriptional regulation would be useful in studying and modeling natural systems or implementing artificial behaviors.

Here, we present a flexible toolkit that integrates mammalian and bacterial RNA-based regulatory mechanisms to create complex synthetic circuit topologies and to regulate endogenous promoters. We combined multiple mammalian RNA processing strategies, including 3′ RNA triple helixes (triplexes) (Wilusz et al., 2012), introns, and ribozymes with mammalian miRNA regulation, bacteria-derived CRISPR-TFs, and the Csy4 RNA-modifying protein. We used these tools to generate functional gRNAs from RNAP-II-regulated mRNAs in human cells for activating both synthetic and endogenous promoters, while rendering the concomitant translation of the harboring mRNAs tunable. Furthermore, we developed strategies for multiplexed gRNA production that enable compact encoding of proteins and multiple gRNAs in single transcripts. To demonstrate the utility of these tools, we implemented multistage transcriptional cascades and combined mammalian miRNA-based regulation with CRISPR-TFs to create multicomponent genetic circuits whose feedback loops, interconnections, and behaviors could be rewired by Csy4-based RNA processing. Thus, integration of CRISPR-TFs with mammalian RNA regulatory architectures can be used to construct complex, synchronized, and switchable networks using synthetic transcriptional regulation and RNA-processing mechanisms.

RESULTS

Functional gRNA Generation with an RNA Triple Helix and Csy4

An important first step to enabling complex CRISPR-TF-based circuits is to generate functional gRNAs from RNAP II promoters in human cells, which would allow for the coupling of gRNA production to specific regulatory signals. For example, the activation of gRNA-dependent circuits could be conditionally initiated in defined cell types or states or tuned in response to external inputs with specific RNAP II promoters. Furthermore, the ability to simultaneously express gRNAs along with proteins from a single transcript would allow multiple outputs, including effector proteins and regulatory links, to be produced from a concise genetic architecture. Thus, we sought to simultaneously generate functional gRNAs and proteins from RNAP II promoters.

We first utilized the RNA-binding and RNA endonuclease capabilities of Csy4 (Haurwitz et al., 2012; Sternberg et al., 2012) to release gRNAs from transcripts that also encode functional protein sequences, generated by RNAP II promoters. Csy4 recognizes a 28 nt RNA sequence (hereafter referred to as the "28" sequence), cleaves the RNA, and remains bound to the upstream RNA fragment (Haurwitz et al., 2012). Specifically, we used the CMV promoter (CMVp) to express a gRNA (gRNA1), flanked by two Csy4 binding sites, downstream of an *mKate2* coding region (Figure 1A). In this architecture, RNA cleavage by Csy4 releases a functional gRNA but also removes the poly-(A) tail from the upstream mRNA, which is known to result in impaired translation of most eukaryotic mRNAs (Proudfoot, 2011).

To complement the Csy4-mediated loss of the poly-(A) tail, we cloned a 110 bp fragment derived from the 3′ end of the mouse MALAT1 locus (Wilusz et al., 2012) downstream of *mKate2* and immediately upstream of the gRNA sequence flanked by Csy4 recognition sites. This sequence forms a highly conserved 3′ triple helical structure known to stabilize transcripts lacking a poly-(A) tail and enables their translation, (Wilusz et al., 2012). Thus, our final "triplex/Csy4" architecture was a CMVp-driven *mKate2* transcript with a 3′ triplex sequence followed by a 28-gRNA-28 sequence (CMVp-*mK*-Tr-28-gRNA-28) (Figure 1A).

To characterize gRNA activity, we cotransfected HEK293T cells with the CMVp-*mK*-Tr-28-gRNA1-28 expression plasmid, along with a plasmid encoding a synthetic P1 promoter that is specifically activated by the gRNA1/taCas9 complex to express *EYFP* (see taCas9 definition below) (Farzadfard et al., 2013). In this experiment and all the following ones (unless otherwise indicated), we also cotransfected a plasmid expressing a transcriptionally active dCas9-NLS-VP64 protein (taCas9), which consists of dCas9 fused to a SV40 nuclear localization signal (NLS) (Kalderon et al., 1984) and the viral VP64 transcription activation domain, which efficiently recruits RNA Pol II to initiate transcription (Beerli et al., 1998). We also transfected HEK293T cells with 0–400 ng of a Csy4-producing plasmid (where Csy4 was produced by the murine PGK1 promoter) along with 1 μg of the other plasmids (Figures 1B and S1A, available online, for raw data).

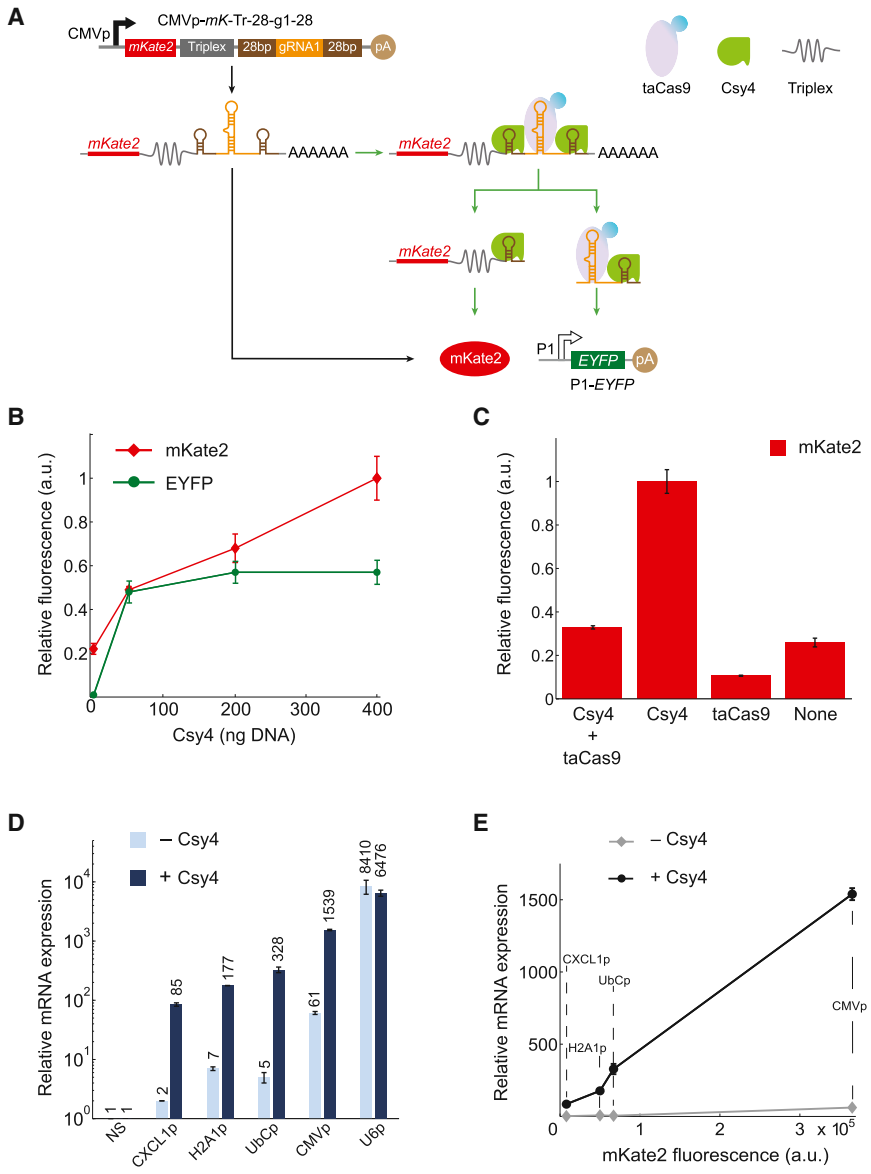

Figure 1. The "Triplex/Csy4" Architecture (CMVp-*mK*-Tr-28-g1-28) Produces Functional gRNAs from RNAP II Promoters while Maintaining Expression of the Harboring Gene

(A) gRNA1 was flanked by two Csy4 recognition sites ("28"), placed downstream of an *mKate2* gene followed by an RNA triplex, and produced by CMVp. Csy4 generates gRNAs that can be incorporated into a transcriptionally active dCas9-VP64 (taCas9) to activate a synthetic promoter (P1) driving *EYFP* (P1-*EYFP*).

(B) The presence of Csy4 enabled a 60-fold increase in EYFP levels, validating the generation of functional gRNAs. Fluorescence values were normalized to the maximum respective fluorescence between the data in this figure and Figures 2B–2D to enable cross-comparisons between the "triplex/Csy4" and "intron/Csy4" architectures.

(C) Csy4 and taCas9 have opposite effects on mKate2 fluorescence generated by CMVp-*mK*-Tr-28-g1-28. The mKate2 fluroescence levels were normalized to the maximum mKate2 value observed (Csy4 only) across the four conditions tested here.

(D) The human RNAP II promoters CXCL1, H2A1, and UbC and the viral CMVp were used to drive expression of four different gRNAs (gRNA3–gRNA6, Table S2) previously shown to activate the *IL1RN* promoter (Perez-Pinera et al., 2013) from the "triplex/Csy4" construct. These results were compared to the RNAP III promoter U6p driving direct expression of the same gRNAs. Four different plasmids, each containing one of the indicated promoters and gRNAs 3–6, were cotransfected along with a plasmid encoding taCas9 and with or without a plasmid expressing Csy4. Relative *IL1RN* mRNA expression, compared to a control construct with nonspecific gRNA (NS, CMVp-*mK*-Tr-28-g1-28), was monitored using qRT-PCR.

(E) The input-output transfer curve for the activation of the endogenous *IL1RN* loci by the "triplex/Csy4" construct was determined by plotting the mKate2 levels (as a proxy for the input) versus the relative *IL1RN* mRNA expression levels (as the output). Tunable modulation of endogenous loci can be achieved with RNAP II promoters of different strengths, with the presence of Csy4 greatly increasing activation compared with the absence of Csy4. The *IL1RN* data is the same as shown in (D). Data are represented as mean ±SEM. See also Figures S1 and S2.

Increasing Csy4 plasmid concentrations increased mKate2 levels by up to 5-fold (Figure 1B). Furthermore, functional gRNAs generated from this construct induced *EYFP* expression by up to 60-fold from the P1 promoter. While *mKate2* expression continued to increase with the concentration of the Csy4-producing plasmid, *EYFP* activation plateaued after 50 ng of the Csy4-producing plasmid. Examination of cell cultures with microscopy showed visual evidence of Csy4-mediated cytotoxicity (roughly ~20% cell death) at 400 ng Csy4 plasmid concentrations while minimal cytotoxicity was observed at 0–200 ng Csy4 plasmid concentrations. Thus, we used 100–200 ng of the Csy4 plasmid in subsequent experiments (except where otherwise noted), although this reduced the number of Csy4-positive cells after transfection. This issue could be addressed in future work by using weaker promoters to regulate Csy4 expression or by generating stable Csy4-producing cell lines.

We characterized the relative effects of Csy4 and taCas9 in this architecture on the levels of the gRNA-harboring protein by measuring mKate2 fluorescence in the presence of Csy4 and taCas9, Csy4 alone, taCas9 alone, or neither protein (Figures 1C and S2A). The lowest mKate2 fluorescence resulted from the taCas9-only condition. Since we used a taCas9 with a strong NLS, this effect could have been mediated by taCas9 binding to the gRNA within the mRNA and localizing the transcript to the nucleus, thus inhibiting translation of the harboring *mKate2*. This hypothesis is supported by data demonstrating that endogenous promoters can be activated by gRNAs produced from the "triplex/Csy4"-based architecture even in

the absence of Csy4 (see below and Figures 1D and 1E). The highest mKate2 levels were obtained with Csy4 alone, suggesting that Csy4 processing could enhance mKate2 levels. The levels of mKate2 in the absence of both Csy4 and taCas9, as well as in the presence of both Csy4 and taCas9, were similar and were reduced by 3- to 4-fold compared with Csy4 only. Thus, titrating Csy4 and taCas9 levels can tune the input-output relationship of CRISPR/Cas-based circuits.

Modulating Endogenous Loci with CRISPR-TFs Expressed from Human Promoters

To validate the robustness of the "triplex/Csy4" architecture, we adapted it to regulate the expression of a native genomic target in human cells. We targeted the endogenous *IL1RN* locus for gene activation via the coexpression of four distinct previously described gRNAs: gRNA3, gRNA4, gRNA5, and gRNA6 (Table S2) (Perez-Pinera et al., 2013). The *IL1RN* gene cluster encodes the expression of IL-1Ra protein, which is a modulator of the immune response and has been shown to be beneficial for treating inflammatory diseases (Dinarello, 2009).

We designed each of the four gRNAs to be expressed concomitantly with mKate2, each from a separate plasmid. Each set of four gRNAs was regulated by one of the following promoters: the CMVp, human Ubiquitin C (UbCp), human Histone H2A1 (H2A1p) (Rogakou et al., 1998), and human inflammatory chemokine CXCL1 (CXCL1p) promoters (Wang et al., 2006). H2A1p and CXCL1p have been shown to be deregulated in a malignant transformation model (Milyavsky et al., 2005). As a control, we also used the RNAP III promoter U6 (U6p) to drive expression of the four gRNAs. For each promoter tested, four plasmids encoding the four different gRNAs were cotransfected along with plasmids expressing taCas9 and Csy4. As a negative control, we substituted the *IL1RN*-targeting gRNA expression plasmids with plasmids that expressed gRNA1, which is nonspecific for the IL1RN promoter (Figure 1D, "NS").

We used qRT-PCR to quantify the mRNA levels of the endogenous *IL1RN* gene, with the results normalized to the nonspecific control. With the four gRNAs regulated by U6p, *IL1RN* activation levels were increased by 8,410-fold in the absence of Csy4 and 6,476-fold with 100 ng of the Csy4-producing plasmid (Figure 1D, "U6p"). *IL1RN* activation with gRNAs expressed from the CMVp was substantial (Figure 1D, "CMVp"), with 61-fold enhancement in the absence of Csy4 and 1,539-fold enhancement in the presence of Csy4. The human RNAP II promoters generated ~2- to 7-fold activation in the absence of Csy4 and ~85- to 328-fold activation in the presence of Csy4 (Figure 1D; "CXCL1p," "H2A1p," and "UbCp"). Strikingly, *IL1RN* activation observed in the absence of Csy4 suggests that taCas9 can utilize gRNAs encoded in long nonprocessed RNA transcripts, albeit with much lower efficiency than Csy4-processed gRNAs.

To characterize the input-output transfer function for endogenous gene regulation, we used mKate2 fluorescence generated by each promoter as a marker of input promoter activity for the various RNAP II promoters (Figure 1E). These data indicate that *IL1RN* activation was not saturated in the conditions tested and that a large dynamic range of endogenous gene regulation can be achieved with human RNAP II promoters. Thus, tunable modulation of native genes can be achieved using CRISPR-TFs with gRNAs expressed from the "triplex/Csy4" architecture.

Functional gRNA Generation from Introns with Csy4

Complementary to the "triplex/Csy4" architecture, we developed an alternative strategy for generating functional gRNAs from RNAP II promoters by encoding gRNAs within an intronic sequence of a gene. Such a strategy has been used previously to generate synthetic siRNAs in mammalian cells (Greber et al., 2008). Specifically, we encoded a gRNA as an intron within the *mKate2* coding sequence using previously described "consensus" acceptor, donor, and branching sequences (Smith et al., 1989; Taggart et al., 2012). We expected that, once spliced, the gRNA would associate with taCas9 to activate a cognate synthetic promoter regulating *EYFP*. However, this simple architecture resulted in undetectable EYFP levels (Figure S2B, bottom panel). These data are consistent with previous studies highlighting that the lifetime of most intronic RNAs is typically only a few minutes (Audibert et al., 2002; Clement et al., 1999). Thus, we concluded that without any stabilization, intronic gRNAs would be expected to be rapidly degraded.

We tried two different approaches to stabilize intronic gRNAs. First, we used intronic sequences that have been reported to produce long-lived introns. This included constructs such as the HSV-1 latency-associated intron, which forms a stable circular intron (Block and Hill, 1997), and the sno-lncRNA2 (snoRNA2) intron, which is processed on both ends by the snoRNA machinery, which protects it from degradation (Yin et al., 2012). However, these approaches also resulted in undetectable activation of the target promoter (data not shown).

As an alternative strategy, we sought to stabilize intronic gRNAs by flanking the gRNA cassette with two Csy4 recognition sites (Figure 2A). In this model, spliced gRNA-containing introns should be bound by Csy4, which should release functional gRNAs. However, Csy4 can also potentially bind and digest the pre-mRNA before splicing occurs. In this case, functional gRNA would be produced, but the *mKate2*-containing pre-mRNA would be degraded in the process (Figure 2A). Thus, increased Csy4 concentrations are expected to result in decreased mKate2 levels but higher levels of functional gRNA. The decrease in mKate2 levels and the increase in functional gRNA levels with Csy4 concentrations could be expected to depend on several factors, which are illustrated in Figure 2A (black arrows, Csy4-independent processes; green arrows, Csy4-mediated processes). These competing factors include the rate at which Csy4 binds to its target sites and cleaves the RNA, the rate of splicing, and the rate of spliced gRNA degradation in the absence of Csy4. To examine the behavior of the "intron/Csy4" architecture, we used CMVp to drive expression of *mKate2* harboring HSV1, snoRNA, and consensus introns containing gRNA1 flanked by two Csy4 binding sites (CMVp-mK_{EX1}-$[28\text{-}g1\text{-}28]_{intron}$-$mK_{EX2}$) along with a synthetic P1 promoter regulating the expression of *EYFP* (Figure 2A).

The presence of Csy4 generated functional gRNA1, as determined by *EYFP* activation (Figures 2B–2D and S1B for raw data). gRNA1 generated from the HSV1 intron produced the strongest *EYFP* activation (Figure 2D), which reached saturation at 200 ng of the Csy4 plasmid. Further experiments with the

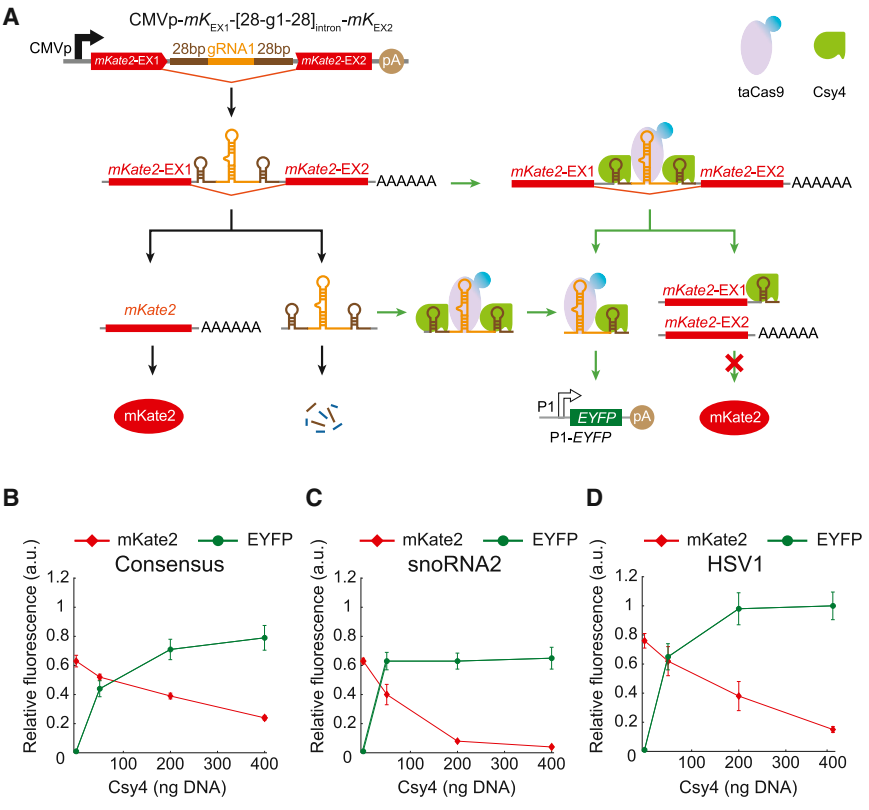

Figure 2. The "Intron/Csy4" Architecture (CMVp-*mK*$_{EX1}$-[28-g1-28]$_{intron}$-*mK*$_{EX2}$) Generates Functional gRNAs from Introns in RNAP-II-Expressed Transcripts

(A) gRNA1 is flanked by Csy4 recognition sites and encoded within an intron, leading to functional gRNA1 generation with Csy4 and activation of a downstream P1-*EYFP* construct. In contrast to the "triplex/Csy4" construct in Figure 1, the "intron/Csy4" architecture results in decreased expression of the harboring gene with increased Csy4 levels, which may be due to cleavage of pre-mRNA prior to splicing.

(B–D) Three introns—a consensus intron (B), snoRNA2 intron (C), and an HSV1 intron (D)—combined with Csy4 resulted in functional gRNAs as assessed by *EYFP* expression. Fluorescence values were normalized to the maximum fluorescence between these data and Figure 1B. Data are represented as mean ±SEM. See also Figures S1–S3.

HSV1 intron showed that while the 5′ Csy4 recognition sequence is important for generating functional intronic gRNAs, the 3′ Csy4 binding site is essential (Figure S3). The snoRNA2 intron saturated *EYFP* expression at 50 ng of the Csy4 plasmid, but the maximal EYFP levels produced by this intron were the lowest of all introns tested (~65% of the HSV1 intron). In addition, increased Csy4 levels concomitantly reduced mKate2 levels. The snoRNA2 intron exhibited the largest decrease in mKate2 levels with increasing Csy4 plasmid concentrations, with a 15-fold reduction in mKate2 fluorescence at 400 ng of the Csy4 plasmid compared to the no Csy4 condition (Figure 2C). The consensus and HSV1 introns exhibited mKate2 levels that were less sensitive to increased Csy4 levels (Figures 2B and 2D). Thus, together with the "triplex/Csy4" architecture, the "intron/Csy4" approach provides a set of parts for tuning the production of functional gRNAs, harboring genes, and regulating downstream targets.

Functional gRNA Generation with *Cis*-Acting Ribozymes

Very recently, the generation of gRNAs from RNAP II promoters for genome editing was demonstrated in wheat (Upadhyay et al., 2013) and yeast (Gao and Zhao, 2014) with *cis*-acting ribozymes. In addition to the "triplex/Csy4"- and "intron/Csy4"-based mechanisms described above, we employed self-cleaving ribozymes to enable gene regulation in human cells via gRNAs generated from RNAP II promoters. Specifically, our gRNAs were engineered to contain a hammerhead (HH) ribozyme (Pley et al., 1994) on their 5′ end and a HDV ribozyme (Ferré-D'Amaré et al., 1998) on their 3′ end (Figure 3).

We tested ribozymes in three different architectures for their ability to generate gRNA1 to activate *EYFP* from P1-*EYFP* and maintain *mKate2* expression: (1) an *mKate2* transcript followed by a triplex and a HH-gRNA1-HDV sequence (CMVp-*mK*-Tr-HH-g1-HDV, Figure 3A); (2) an *mKate2* transcript followed a HH-gRNA1-HDV sequence (CMVp-*mK*-HH-g1-HDV, Figure 3B); and (3) the sequence HH-gRNA1-HDV with no associated protein-coding gene (CMVp-HH-g1-HDV, Figure 3C). We compared gRNAs generated from these architectures with gRNAs produced by U6p and the "triplex/Cys4" architecture (with 200 ng of the Csy4 plasmid).

All constructs that contained *mKate2* exhibited detectable mKate2 fluorescence (Figures 3D and S4). Surprisingly, this included CMVp-*mK*-HH-g1-HDV, which did not have a triplex sequence and was thus expected to have low mKate2 levels due to removal of the poly-(A) tail. Our observations could result from inefficient ribozyme cleavage (Chowrira et al., 1994) that allows nonprocessed transcripts to be transported to the cytoplasm and translated, protection of the *mKate2* transcript by the residual 3′ ribozyme sequence, or other mechanisms yet to be determined. In terms of target *EYFP* activation, the highest EYFP fluorescence level was generated from gRNAs expressed by U6p, followed by the CMVp-HH-g1-HDV and CMVp-*mK*-HH-g1-HDV constructs (Figure 3D). The CMVp-*mK*-Tr-HH-gRNA1-HDV and "triplex/Csy4" architectures resulted in similar EYFP levels. Thus, *cis*-acting ribozymes can mediate functional gRNA expression from RNAP II promoters.

Multiplexed gRNA Expression from Single RNA Transcripts

A major challenge in constructing CRISPR-TF-based circuits in human cells, especially ones that interface with endogenous promoters, is that multiple gRNAs are necessary to achieve desired activation levels, since single gRNAs do not typically achieve significant activation (Cheng et al., 2013; Maeder

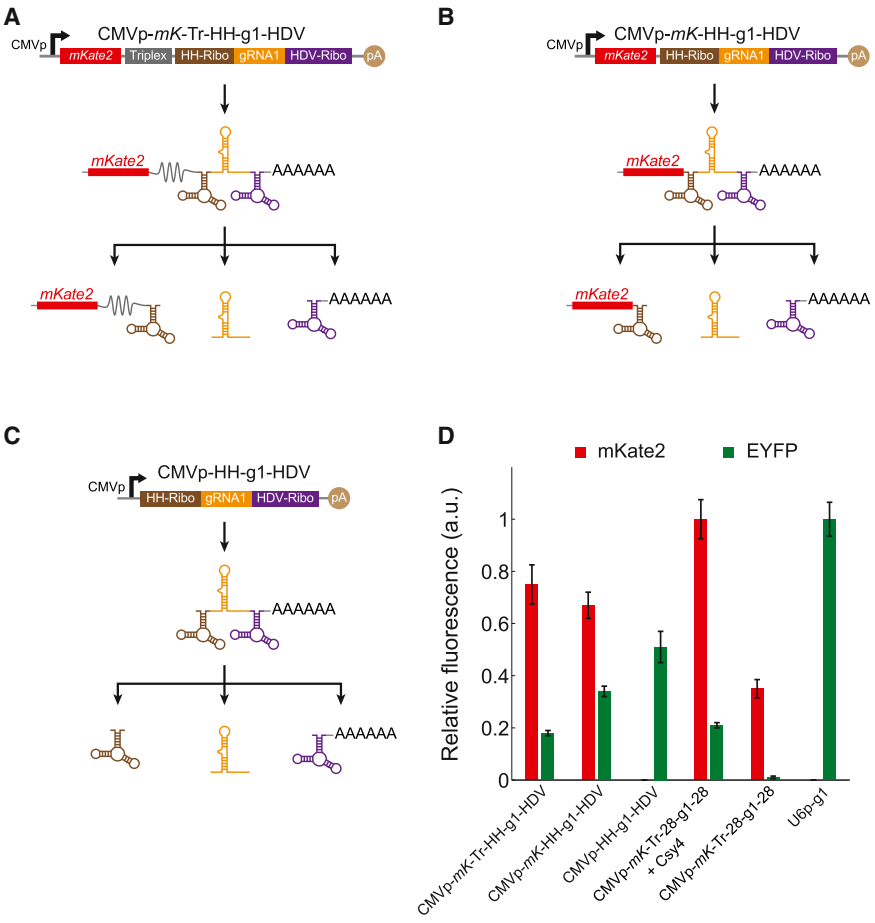

Figure 3. Ribozyme Architectures Expressed from CMVp Can Produce Active gRNAs

(A) gRNA1 was flanked with hammerhead (HH) and HDV ribozymes and encoded downstream of *mKate2* with an RNA triplex (CMVp-*mK*-Tr-HH-g1-HDV).

(B) gRNA1 was flanked with HH and HDV ribozymes and encoded downstream of *mKate2* with no RNA triplex (*mK*-HH-g1-HDV).

(C) gRNA1 was flanked with HH and HDV ribozymes (HH-g1-HDV).

(D) The three architectures efficiently generated gRNA1 to activate P1-*EYFP*. The "triplex/Csy4" construct (CMVp-*mK*-Tr-28-g1-28), with and without Csy4, and the RNAP III promoter U6p driving gRNA1 (U6p-g1) are shown for comparison. Data are represented as mean ±SEM. See also Figure S4.

et al., 2013; Mali et al., 2013a; Perez-Pinera et al., 2013). Current techniques rely on multiple gRNA expression cassettes, each with their own promoter and terminator. Our toolkit can generate multiple functional gRNAs from a single compact transcript.

We expressed two independent gRNAs from a single RNA transcript to activate two independent downstream promoters. In the first architecture ("intron-triplex"), we encoded gRNA1 within an HSV1 intron flanked by two Csy4 binding sites within the coding sequence of *mKate2*. Furthermore, we encoded gRNA2 enclosed by two Csy4 binding sites downstream of the *mKate2*-triplex sequence (Figure 4A, "Input A"). In the second architecture ("triplex-tandem"), we surrounded both gRNA1 and gRNA2 with Csy4 binding sites and placed them in tandem, downstream of the *mKate2*-triplex sequence (Figure 4B, "Input B"). In both architectures, gRNA1 and gRNA2 targeted the synthetic promoters P1-*EYFP* and P2-*ECFP*, respectively.

Both strategies for multiplexed gRNA expression enable functional taCas9 activity at multiple downstream targets and can be tuned for desired applications (Figures 4C and S5). Specifically, the "intron-triplex" construct exhibited a 3-fold decrease in mKate2, a 10-fold increase in EYFP, and a 100-fold increase in ECFP in the presence of 200 ng of the Csy4 plasmid compared to no Csy4. In the "triplex-tandem" architecture, *mKate2*, *EYFP*, and *ECFP* expression increased by 3-fold, 36-fold, and 66-fold, respectively, in the presence of 200 ng of the Csy4 plasmid when compared to no Csy4. The "intron-triplex" architecture had higher EYFP and ECFP levels compared with the "triplex-tandem" architecture. Thus, Csy4 enables the generation of multiple gRNAs from a single mRNA transcript.

To demonstrate the utility of our multiplexing toolkit in targeting endogenous loci, we encoded multiple gRNAs targeting the *IL1RN* promoter into a single transcript. Previously described gRNAs for *IL1RN* activation, separated by Csy4 binding sites, were cloned in tandem, downstream of an *mKate2*-triplex sequence on a single transcript (Figure 5A). We measured *IL1RN* activation by the multiplexed single-transcript construct as well as an architecture where the four different gRNAs were expressed from four different plasmids (Figure 5B, "Multiplexed" versus "Non multiplexed", respectively). In the presence of 100 ng of the Csy4 plasmid, the multiplexed architecture resulted in a ~1,111-fold activation over nonspecific gRNA1 ("NS") compared with ~461-fold for the nonmultiplexed set of single-gRNA-expressing plasmids. Moreover, ~155-fold *IL1RN* activation was detected with the multiplexed architecture even in the absence of Csy4, further supporting our observation that taCas9 can utilize gRNAs encoded in long transcripts, albeit with significantly lower efficiency. Together with Figure 4, these results show that it is possible to generate multiple functional gRNAs for multiplexed expression from a single, concise RNA transcript. These architectures thus enable compact programming of Cas9 function for implementing multioutput synthetic gene circuits, for modulating endogenous genes, and potentially for achieving conditional multiplexed genome editing.

Synthetic Transcriptional Cascades with RNA-Guided Regulation

To demonstrate the utility of our RNA-dependent regulatory toolkit, we used it to create the first CRISPR-TF-based

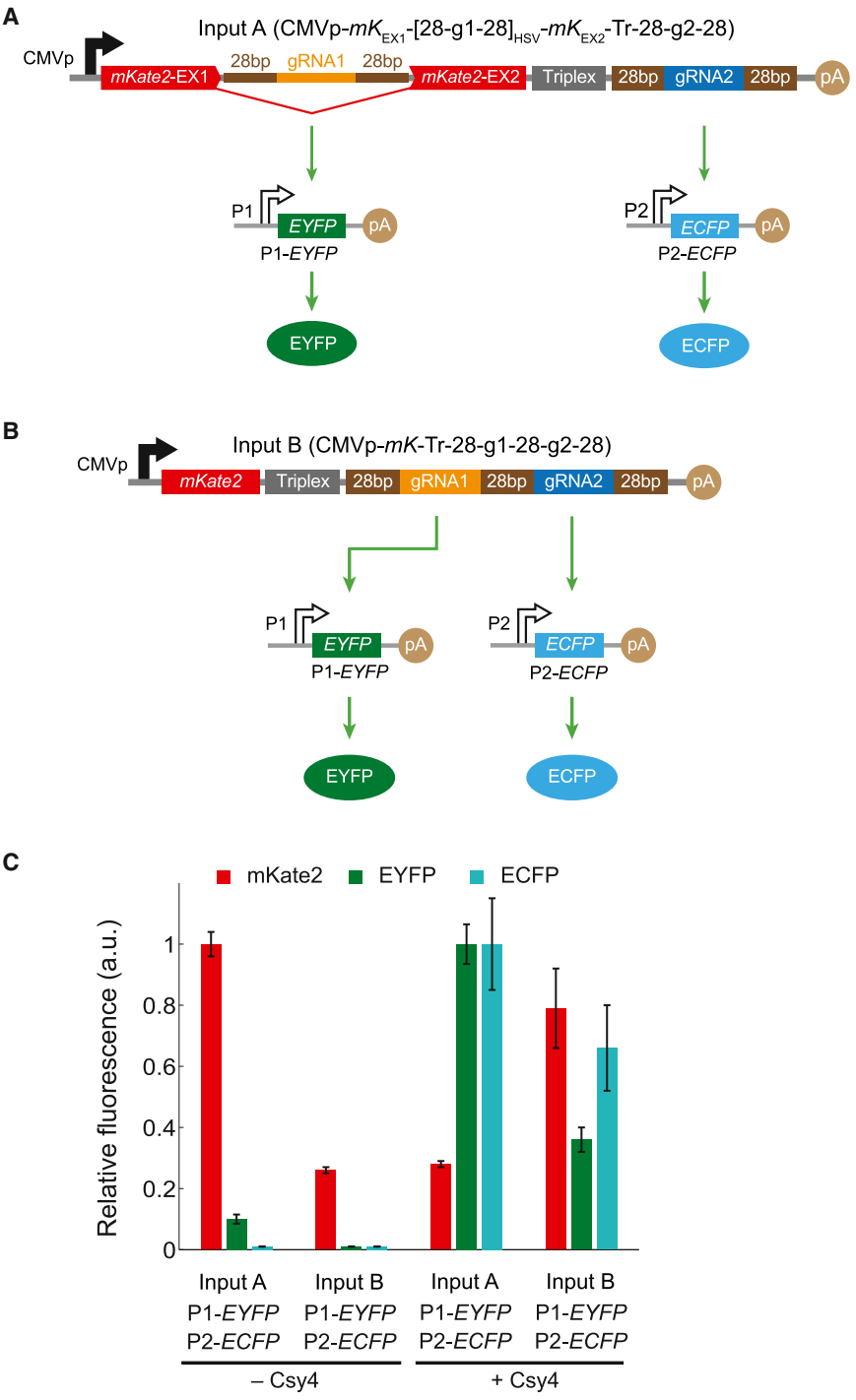

Figure 4. The "Triplex/Csy4" and "Intron/Csy4" Architectures Enable Multiplexed gRNA Expression from a Single Transcript and Compact Encoding of Synthetic Circuits with Multiple Outputs

(A) In the first design (Input A, "intron-triplex"), we encoded gRNA1 within a HSV1 intron and gRNA2 after an RNA triplex. Both gRNAs were flanked by Csy4 recognition sites. Functional gRNA expression was assessed by activation of a gRNA1-specific P1-*EYFP* construct and a gRNA2-specific P2-*ECFP* construct.

(B) In the second design (Input B, "triplex-tandem"), we encoded both gRNA1 and gRNA2 in tandem, with intervening and flanking Csy4 recognition sites, downstream of *mKate2* and an RNA triplex. Functional gRNA expression was assessed by activation of a gRNA1-specific P1-*EYFP* construct and a gRNA2-specific P2-*ECFP* construct.

(C) Both multiplexed gRNA expression constructs efficiently activated *EYFP* and *ECFP* expression in the presence of Csy4, thus demonstrating the generation of multiple active gRNAs from a single transcript. Data are represented as mean ±SEM. See also Figure S5.

transcriptional cascades. Many complex gene circuits require the ability to implement cascades, in which signals integrated at one stage are transmitted to downstream stages for processing and actuation (Ellis et al., 2009; Hooshangi et al., 2005). Furthermore, transcriptional cascades are important in natural regulatory systems, such as those that control segmentation, sexual commitment, and development (Dequéant and Pourquié, 2008; Sinha et al., 2014). However, despite the potential utility of CRISPR-TFs for artificial gene circuits, CRISPR-TF-based cascades have not been built to date.

We integrated the "triplex/Csy4" and "intron/Csy4" strategies to build two different, three-stage CRISPR-TF-mediated transcriptional cascades (Figure 6). In the first design, CMVp-driven expression of gRNA1 from an "intron/Csy4" construct generated gRNA1 from an HSV1 intron, which activated a synthetic promoter P1 to produce gRNA2 from a "triplex/Csy4" architecture, which then activated a downstream synthetic promoter P2 regulating *ECFP* (Figure 6A). In the second design, the intronic gRNA expression cassette in the first stage of the cascade was replaced by a "triplex/Csy4" architecture for expressing gRNA1 (Figure 6B). We tested these two designs in the presence of 200 ng of the Csy4 plasmid (Figures 6C, 6D, and S6).

In the first cascade design, a 76-fold increase in EYFP and a 13-fold increase in ECFP were observed compared to a control in which the second stage of the cascade (P1-*EYFP*-Tr-28-g2-28) was replaced by an empty plasmid (Figure 6C). In the second cascade design, a 31-fold increase in EYFP and a 21-fold increase in ECFP were observed compared to a control in which the second stage of the cascade (P1-*EYFP*-Tr-28-g2-28) was replaced by an empty plasmid (Figure 6D). These results demonstrate that there is minimal nonspecific activation of promoter P2

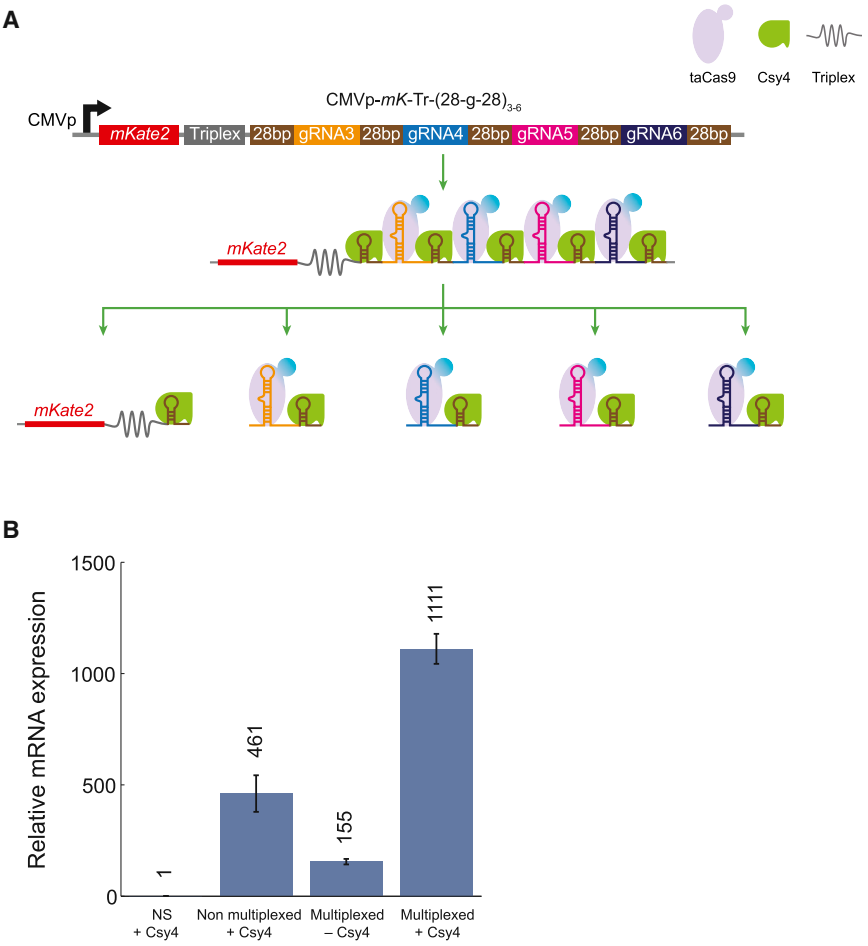

Figure 5. Multiplexed gRNA Expression from a Single, Compact Transcript Enables Efficient Activation of Endogenous Loci

(A) Four different gRNAs (gRNA3–gRNA6) were multiplex-encoded in tandem, with intervening and flanking Csy4 recognition sites, downstream of *mKate2* and an RNA triplex (CMVp-*mK*-Tr-$(28\text{-g-}28)_{3\text{-}6}$).

(B) The multiplexed *mK*-Tr-$(28\text{-g-}28)_{3\text{-}6}$ construct exhibited high-level activation of *IL1RN* expression in the presence of Csy4 compared with the same construct in the absence of Csy4. Relative *IL1RN* mRNA expression was determined based on a control construct with nonspecific gRNA1 (NS, CMVp-*mK*-Tr-28-g1-28) expressed via the "triplex/Csy4" architecture. For comparison, a nonmultiplexed set of plasmids containing the same gRNAs (gRNA3–gRNA6), each produced from separate, individual plasmids (CMVp-*mK*-Tr-28-gRNA-28) with the "triplex/Csy4" architecture is shown. Data are represented as mean ±SEM.

by gRNA1 (see also Figure S2C), which is essential for the scalability and reliability of transcriptional cascades. Furthermore, the activation of each stage in the cascade was dependent on the presence of all upstream nodes, which is expected in properly functioning transcriptional cascades (Figures 6C and 6D).

Rewiring RNA-Dependent Synthetic Regulatory Circuits

We integrated CRISPR-TF regulation with mammalian RNAi to implement more sophisticated circuit topologies and to show how network motifs could be rewired by Csy4-based RNA processing. Specifically, we incorporated miRNA regulation with CRISPR-TFs and used Csy4 to disrupt miRNA inhibition of target RNAs by removing cognate miRNA binding sites. We first built a single RNA transcript that was capable of multiplexed gene regulation by expressing both a functional miRNA (Greber et al., 2008; Xie et al., 2011) and a functional gRNA. This was achieved by encoding a mammalian miRNA inside the consensus intron within the *mKate2* gene, followed by a triplex sequence and a gRNA1 sequence flanked by Csy4 recognition sites (Figure 7A, CMVp-mK_{EX1}-[miR]-mK_{EX2}-Tr-28-g1-28). The first output was a constitutively expressed *ECFP* gene followed by a triplex sequence, a Csy4 recognition site, 8× miRNA binding sites (8× miRNA-BS), and another Csy4 recognition site (Figure 7A). The second output was the P1 promoter regulating *EYFP* (Figure 7A).

In the absence of Csy4, ECFP and EYFP levels were low because the miRNA suppressed *ECFP* expression and no functional gRNA1 was generated (Figures 7B and S7, "Mechanism 1"). In the presence of Csy4, *ECFP* expression increased by 30-fold compared to the no Csy4 condition, which we attributed to Csy4-induced separation of the 8× miRNA-BS from the *ECFP* transcript (Figure 7B). Also, the presence of Csy4 generated functional gRNA1, leading to 17-fold increased *EYFP* expression compared to the no Csy4 condition (Figure 7B). The mKate2 fluorescence levels were high in both the Csy4-positive and Csy4-negative conditions. Thus, Csy4 catalyzed RNA-based rewiring of circuit connections between the input node and its two outputs by simultaneously inactivating a repressive output link and turning on an activating output link (Figure 7C).

To demonstrate facile circuit programming using RNA-dependent mechanisms, we extended the design in Figure 7A by incorporating an additional 4× miRNA-BS at the 3′ end of the *mKate2*-containing transcript (Figure 7D, CMVp-mK_{EX1}-[miR]-mK_{EX2}-Tr-28-g1-28-$miR_{4\times BS}$). In the absence of Csy4, this resulted in autoregulatory, negative-feedback suppression of *mKate2* expression by the miRNA generated within the *mKate2* intron (Figures 7E and S7, "Mechanism 2"). In addition, both ECFP and EYFP levels remained low due to repression of *ECFP* by the miRNA and the lack of functional gRNA1 generation. However, in the presence of Csy4, mKate2 levels increased by 21-fold due to Csy4-mediated separation of the 4× miRNA-BS from the *mKate2* transcript. Furthermore, *ECFP* inhibition by the miRNA was relieved in a similar fashion, resulting in a 27-fold increase in ECFP levels. Finally, functional gRNA1 was

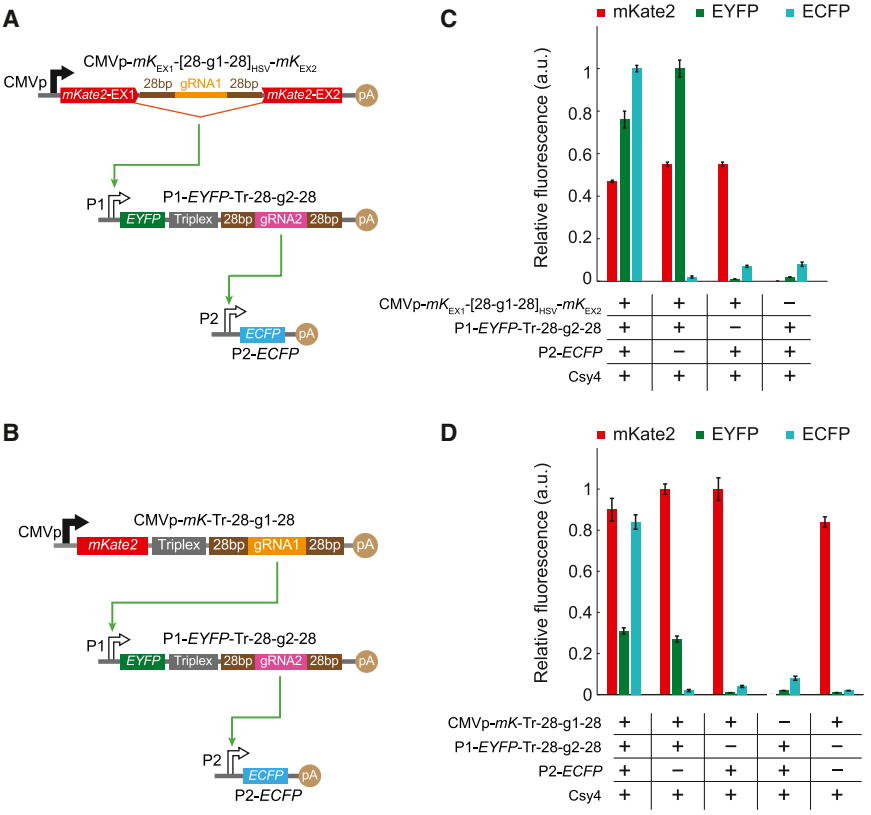

Figure 6. Multistage Transcriptional Cascades Can Be Implemented with Our CRISPR-TF Architectures

(A) A three-stage transcriptional cascade was implemented by using intronic gRNA1 (CMVp-mK_{EX1}-[28-g1-28]$_{HSV}$-mK_{EX2}) as the first stage. gRNA1 specifically targeted the P1 promoter to express gRNA2 (P1-*EYFP*-Tr-28-g2-28), which then activated expression of *ECFP* from the P2 promoter (P2-*ECFP*).

(B) A three-stage cascade was implemented by using a "triplex/Csy4" architecture to express gRNA1 (CMVp-*mK*-Tr-28-g1-28). gRNA1 specifically targeted the P1 promoter to express gRNA2 (P1-*EYFP*-Tr-28-g2-28), which then activated expression of *ECFP* from P2 (P2-*ECFP*).

(C and D) The complete three-stage cascade from (A) and (B), respectively, exhibited expression of all three fluorescent proteins. The removal of one of each of the three stages in the cascade resulted in the expected loss of fluorescence of the specific stage and dependent downstream stages. The control condition in column 4 in (C) and (D) are duplicated, since the two circuits in (A) and (B) were tested in the same experiment. Data are represented as mean ±SEM. See also Figure S6.

generated, leading to a 50-fold increase in EYFP levels (Figure 7E). Thus, Csy4 catalyzed RNA-based rewiring of circuit connections between the input node and its two outputs by simultaneously inactivating a repressive output link, turning on an activating output link, and inactivating an autoregulatory feedback loop (Figure 7F).

DISCUSSION

Synthetic biology provides tools for studying basic biology by disrupting, rewiring, and mimicking natural network motifs (Elowitz and Lim, 2010). In addition, synthetic circuits have been used to link exogenous signals to endogenous gene regulation (Fussenegger et al., 2000; Ye et al., 2011), to address biomedical applications (Nissim and Bar-Ziv, 2010; Weber and Fussenegger, 2012), and to perform cellular computation (Benenson, 2012; Daniel et al., 2013; Nissim et al., 2007). Although many synthetic gene circuits have been based on transcriptional regulation, RNA-based regulation has also been used to construct a variety of artificial gene circuits (Ausländer et al., 2012; Benenson, 2012; Saito et al., 2010; Xie et al., 2011). However, previous efforts have not yet integrated RNA-based regulation with CRISPR-TFs, which are both promising strategies for implementing scalable genetic circuits given their programmability and potential for multiplexing.

In this work, we created a rich toolkit for engineering artificial gene circuits and endogenous gene regulation in human cells. We developed multiple complementary approaches to generate functional gRNAs from transcripts of translated genes regulated by RNAP II promoters. These architectures, based either on Csy4 or ribozymes, enable the encoded RNA and protein levels to be tuned. Choosing between these architectures depends on the specific application. When gRNA expression does not need to be specifically timed or synchronized in a complex fashion, a constitutively active ribozyme-based system is beneficial, since it does not need the expression of an additional protein (Csy4). Conditional gRNA production via ribozyme-based architectures can be achieved by using conditional RNAP II promoters or ligand-dependent cleavage (Soukup and Breaker, 1999) to trigger gRNA release using exogenous control. Applications that require more complicated regulation, synchronization or rewiring of multiple genes (Figure 7), and/or tunable input-output relationships can benefit from the additional control afforded by Csy4. For example, functional gRNAs are produced with the expression of the harboring RNA transcript and the presence of Csy4. The expression of both of these components could be linked to regulated or conditional promoters for more specific spatial or temporal control of CRISPR-TF circuits.

Complementary to synthetic circuits, we showed that this toolkit can be used to activate endogenous promoters from multiple different endogenous human RNAP II promoters, as well as viral CMVp. We also described useful strategies for multiplexed gRNA expression from compact single transcripts to modulate both synthetic and native promoters. This feature is beneficial because it can be used to regulate multiple nodes from a single concise one, thus enabling sophisticated circuits with a large number of parallel "fan-outs" (i.e., outgoing interconnections from a given node) and networks with dense

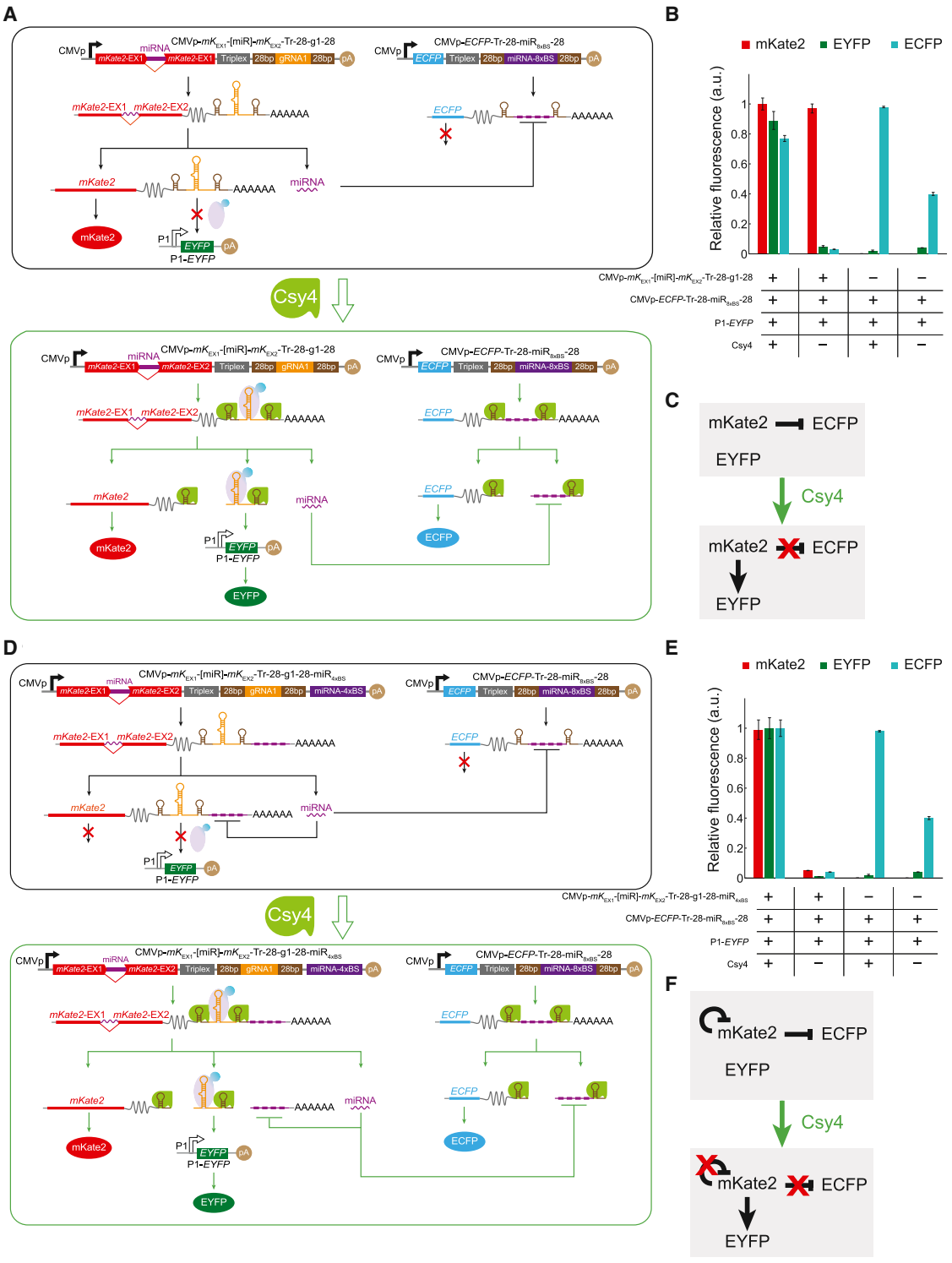

Figure 7. CRISPR-Based Transcriptional Regulation Can Be Integrated with Mammalian miRNAs and RNA Processing Mechanisms as well as with Csy4-Dependent RNA Processing to Implement Feedback Loops and Multioutput Circuits that Can Be Rewired at the RNA Level

(A) We created a single transcript that encoded both miRNA and CRISPR-TF regulators by expressing a miRNA from an intron within *mKate2* and gRNA1 from a "triplex/Csy4" architecture (CMVp-mK_{EX1}-[miR]-mK_{EX2}-Tr-28-g1-28). In the presence of taCas9, but in the absence of Csy4, this circuit did not activate a downstream gRNA1-specific P1-*EYFP* construct and did repress a downstream *ECFP* transcript with 8× miRNA binding sites flanked by Csy4 recognition sites (CMVp-*ECFP*-Tr-28-$miR_{8\times BS}$). In the presence of both taCas9 and Csy4, this circuit was rewired by activating gRNA1 production and subsequent *EYFP* expression, as well as by separating the *ECFP* transcript from the 8× miRNA binding sites, thus ablating miRNA inhibition of ECFP expression.

(legend continued on next page)

interconnections. Moreover, the ability to target endogenous loci with several gRNAs in a condensed fashion is critical, since multiple gRNAs are needed for substantial modulation of native promoters. Thus, our tools can be used to build efficient artificial gene networks and to perturb native regulatory networks.

The native CRISPR RNA context can be used for multiplexed genome engineering when expressed from RNAP III promoters in mammalian cells (Cong et al., 2013). However, it remains unclear whether CRISPR/Cas-based systems can be multiplexed when expressed from RNAP II promoters using this approach and what cellular factors mediate this process. In addition to transcriptional regulation, if a nuclease-proficient Cas9 was used with our platform instead of taCas9, then in vivo multiplexed genome editing activity could be conditionally linked to cellular signals via regulation of gRNA expression. In addition to genetic studies, this capability could be potentially used to create in vivo DNA-based "ticker tapes" that link cellular events to mutations.

This framework integrates mammalian RNA regulatory mechanisms with the RNA-dependent protein, dCas9, and the RNA-processing protein, Csy4, from bacteria. These architectures lay a foundation for sophisticated and compact synthetic gene circuits in human cells, such as multistage, multi-input/multi-output networks and feedback circuits capable of logic, computing, and interfacing with endogenous systems. Theoretically, since the specificity of regulatory interconnections with these tools is determined only by RNA sequences, scalable circuits with almost any network topology could be constructed. We demonstrated highly specific and effective three-layer transcriptional cascades with two different architectures that incorporated RNA triplexes, introns, Csy4, and CRISPR-TFs. The absence of undesired crosstalk between different stages of the cascade underscores the orthogonality and scalability of RNA-dependent regulatory schemes.

We also combined RNA regulatory parts, CRISPR-TFs, and RNAi to create various circuit topologies that can be rewired via conditional RNA processing. Since both positive and negative regulation are possible with the same taCas9 protein (Farzadfard et al., 2013) and miRNAs enact tunable negative regulation, many important multifunctional and multicomponent network topologies can be implemented using this set of regulatory parts. In addition, Csy4 can be used to catalyze changes in gene expression by modifying RNA transcripts and rewiring network topologies. For example, functional gRNAs were liberated for transcriptional modulation, and miRNA binding sites were removed from RNA transcripts to eliminate miRNA-based links. This mechanism demonstrates the potential of adapting bacterial proteins to modulate mammalian gene regulation at the RNA level. This feature could be used to minimize unwanted leakage in positive feedback loops and to dynamically switch circuits between different states. By linking Csy4 expression to endogenous promoters, interconnections between circuits and network behavior could also be conditionally linked to specific tissues, events (e.g., cell cycle phase and mutations), or environmental conditions. With genome mining or directed mutagenesis, orthogonal Cas9 and Csy4 variants could be discovered and used for more complicated regulatory and RNA processing schemes (Esvelt et al., 2013).

In summary, this work provides a diverse set of tools for constructing scalable regulatory gene circuits, tuning them, modifying connections between circuit components, and synchronizing the expression of multiple genes in a network. Furthermore, these regulatory parts could be used to interface synthetic gene circuits with endogenous systems as well as to rewire endogenous networks. Importantly, the promoters, proteins, and miRNAs used in these architectures are not limited to synthetic ones. For many applications, it will be useful to utilize endogenous cellular components, such as tissue- or cell-phase-specific promoters and miRNAs, in order to interface engineered systems with native networks. Similarly, the outputs for these architectures are not limited to reporter genes, but can be effector genes, multiplexed gRNAs that target endogenous promoters, or any other encodable gene. We envision that integrating RNA-dependent regulatory mechanisms with RNA processing will enable sophisticated transcriptional and post-transcriptional regulation, accelerate synthetic biology, and facilitate the study of basic biology in human cells.

EXPERIMENTAL PROCEDURES

Plasmid Construction

The CMVp-*dCas9-3×NLS-VP64* (taCas9, Construct 1, Table S1) plasmid was built as described previously (Farzadfard et al., 2013). The *csy4* gene from *P. aeruginosa* strain UCBPP-PA14 (Qi et al., 2012) was codon optimized for expression in human cells and cloned downstream of the PGK1 promoter in a PGK1p-*EBFP2* plasmid (Farzadfard et al., 2013) to create PGK1p-*Csy4*-pA (Construct 2, Table S1). The various gRNA expression constructs were built using conventional restriction enzyme cloning, Golden Gate assembly, and/or Gibson assembly (Table S1; Supplemental Experimental Procedures).

Cell Culture and Transfections

Low-passage HEK293T cells were obtained from ATCC; freshly thawed cells were used in this study and were replaced with a fresh batch every 2 months. They were maintained in Dulbecco's modified Eagle's medium (DMEM) supplemented with 10% FBS, 1% penicillin-streptomycin, 1% GlutaMAX, and non-essential amino acids at 37°C with 5% CO_2. HEK293T cells were transfected with FuGENE®HD Transfection Reagent (Promega) according to the manufacturer's instructions. Each transfection was made using 200,000 cells/well in a 6-well plate. As a control, with 2 μg of a single plasmid in which a CMVp regulated *mKate2*, transfection efficiencies were routinely higher than 90% (determined by flow cytometry). Unless otherwise indicated, each

(B and C) Csy4 production changes the behavior of the circuit in (A) by rewiring circuit interconnections.
(D) We incorporated an autoregulatory feedback loop into the network topology of the circuit described in (A) by encoding 4× miRNA binding sites at the 3′ end of the input transcript (CMVp-mK_{EX1}-[miR]-mK_{EX2}-Tr-28-g1-28-$miR_{4\times BS}$). This negative feedback suppressed *mKate2* expression in the absence of Csy4. However, in the presence of Csy4, the 4× miRNA binding sites were separated from the *mKate2* mRNA, thus leading to *mKate2* expression.
(E and F) Csy4 production changes the behavior of the circuit in (D) by rewiring circuit interconnections. In contrast to the circuit in (A), *mKate2* was suppressed in the absence of Csy4 but was highly expressed in the presence of Csy4 due to elimination of the miRNA-based autoregulatory negative feedback. Each of the mKate2, EYFP, and ECFP levels in (B) and (E) were normalized to the respective maximal fluorescence among all tested scenarios. The controls in column 3 and 4 in (B) and (E) are duplicated, since the two circuits in (A) and (D) were tested in the same experiment with the same controls. Data are represented as mean ±SEM. See also Figure S7.

plasmid was transfected at 1 μg/sample. All samples were transfected with taCas9, unless specifically indicated. Cells were processed for flow cytometry or qRT-PCR analysis 72 hr after transfection.

Quantitative RT-PCR

The RT-PCR procedure was developed in Perez-Pinera et al. (2013) and described in Supplemental Experimental Procedures. Reported values are the means of three independent biological replicates with technical duplicates that were averaged for each experiment. Error bars represent SEM.

Flow Cytometry

Cells were washed with DMEM and 1×PBS, resuspended in 1×PBS, and immediately assayed with a Becton Dickinson LSRII Fortessa flow cytometer. At least 50,000 cells were recorded per sample in each data set. The results of each experiment represent at least three biological replicates. Error bars are SEM on the weighted median fluorescence values (Supplemental Experimental Procedures).

SUPPLEMENTAL INFORMATION

Supplemental Information includes seven figures, two tables, and Supplemental Experimental Procedures and can be found with this article online at http://dx.doi.org/10.1016/j.molcel.2014.04.022.

AUTHOR CONTRIBUTIONS

L.N. and S.P. contributed equally. L.N., S.P., and T.K.L. conceived the work. L.N., S.P., A.F, and P.P. performed experiments. L.N., S.P., P.P., and T.K.L. discussed results and wrote the paper.

ACKNOWLEDGMENTS

We thank members of the Lu lab, especially Ramiz Daniel and Ky Lowenhaupt, for helpful discussions. We thank Lila Wroblewska for an *mKate2* plasmid expressing intronic miRNA and Jeremy Wilusz and Courtney JnBaptiste for the *cGFP*_MALAT1_3′ plasmid. L.N. would like to thank Dr. Adina Binder-Nissim for support. This work was supported by the Defense Advanced Research Projects Agency and the National Institutes of Health (DP2 OD008435 and P50 GM098792).

Received: March 22, 2014
Revised: April 15, 2014
Accepted: April 18, 2014
Published: May 15, 2014

REFERENCES

Audibert, A., Weil, D., and Dautry, F. (2002). In vivo kinetics of mRNA splicing and transport in mammalian cells. Mol. Cell. Biol. *22*, 6706–6718.

Ausländer, S., Ausländer, D., Müller, M., Wieland, M., and Fussenegger, M. (2012). Programmable single-cell mammalian biocomputers. Nature *487*, 123–127.

Beerli, R.R., and Barbas, C.F., 3rd. (2002). Engineering polydactyl zinc-finger transcription factors. Nat. Biotechnol. *20*, 135–141.

Beerli, R.R., Segal, D.J., Dreier, B., and Barbas, C.F., 3rd. (1998). Toward controlling gene expression at will: specific regulation of the erbB-2/HER-2 promoter by using polydactyl zinc finger proteins constructed from modular building blocks. Proc. Natl. Acad. Sci. USA *95*, 14628–14633.

Benenson, Y. (2012). Biomolecular computing systems: principles, progress and potential. Nat. Rev. Genet. *13*, 455–468.

Block, T.M., and Hill, J.M. (1997). The latency associated transcripts (LAT) of herpes simplex virus: still no end in sight. J. Neurovirol. *3*, 313–321.

Blount, B.A., Weenink, T., Vasylechko, S., and Ellis, T. (2012). Rational diversification of a promoter providing fine-tuned expression and orthogonal regulation for synthetic biology. PLoS ONE *7*, e33279.

Chen, M., and Manley, J.L. (2009). Mechanisms of alternative splicing regulation: insights from molecular and genomics approaches. Nat. Rev. Mol. Cell Biol. *10*, 741–754.

Chen, X., Wu, J.M., Hornischer, K., Kel, A., and Wingender, E. (2006). TiProD: the Tissue-specific Promoter Database. Nucleic Acids Res. *34* (Database issue), D104–D107.

Cheng, A.A., and Lu, T.K. (2012). Synthetic biology: an emerging engineering discipline. Annu. Rev. Biomed. Eng. *14*, 155–178.

Cheng, A.W., Wang, H., Yang, H., Shi, L., Katz, Y., Theunissen, T.W., Rangarajan, S., Shivalila, C.S., Dadon, D.B., and Jaenisch, R. (2013). Multiplexed activation of endogenous genes by CRISPR-on, an RNA-guided transcriptional activator system. Cell Res. *23*, 1163–1171.

Chowrira, B.M., Pavco, P.A., and McSwiggen, J.A. (1994). In vitro and in vivo comparison of hammerhead, hairpin, and hepatitis delta virus self-processing ribozyme cassettes. J. Biol. Chem. *269*, 25856–25864.

Clement, J.Q., Qian, L., Kaplinsky, N., and Wilkinson, M.F. (1999). The stability and fate of a spliced intron from vertebrate cells. RNA *5*, 206–220.

Cong, L., Ran, F.A., Cox, D., Lin, S., Barretto, R., Habib, N., Hsu, P.D., Wu, X., Jiang, W., Marraffini, L.A., and Zhang, F. (2013). Multiplex genome engineering using CRISPR/Cas systems. Science *339*, 819–823.

Cronin, C.A., Gluba, W., and Scrable, H. (2001). The lac operator-repressor system is functional in the mouse. Genes Dev. *15*, 1506–1517.

Daniel, R., Rubens, J.R., Sarpeshkar, R., and Lu, T.K. (2013). Synthetic analog computation in living cells. Nature *497*, 619–623.

Dequéant, M.L., and Pourquié, O. (2008). Segmental patterning of the vertebrate embryonic axis. Nat. Rev. Genet. *9*, 370–382.

Dinarello, C.A. (2009). Immunological and inflammatory functions of the interleukin-1 family. Annu. Rev. Immunol. *27*, 519–550.

Ellis, T., Wang, X., and Collins, J.J. (2009). Diversity-based, model-guided construction of synthetic gene networks with predicted functions. Nat. Biotechnol. *27*, 465–471.

Elowitz, M., and Lim, W.A. (2010). Build life to understand it. Nature *468*, 889–890.

Esvelt, K.M., Mali, P., Braff, J.L., Moosburner, M., Yaung, S.J., and Church, G.M. (2013). Orthogonal Cas9 proteins for RNA-guided gene regulation and editing. Nat. Methods *10*, 1116–1121.

Farzadfard, F., Perli, S.D., and Lu, T.K. (2013). Tunable and Multifunctional Eukaryotic Transcription Factors Based on CRISPR/Cas. ACS Synth. Biol. *2*, 604–613.

Ferré-D'Amaré, A.R., Zhou, K., and Doudna, J.A. (1998). Crystal structure of a hepatitis delta virus ribozyme. Nature *395*, 567–574.

Fussenegger, M., Morris, R.P., Fux, C., Rimann, M., von Stockar, B., Thompson, C.J., and Bailey, J.E. (2000). Streptogramin-based gene regulation systems for mammalian cells. Nat. Biotechnol. *18*, 1203–1208.

Gao, Y., and Zhao, Y. (2014). Self-processing of ribozyme-flanked RNAs into guide RNAs in vitro and in vivo for CRISPR-mediated genome editing. J. Integr. Plant Biol. *56*, 343–349.

Gauthier, N.P., Jensen, L.J., Wernersson, R., Brunak, S., and Jensen, T.S. (2010). Cyclebase.org: version 2.0, an updated comprehensive, multi-species repository of cell cycle experiments and derived analysis results. Nucleic Acids Res. *38* (Database issue), D699–D702.

Gilbert, L.A., Larson, M.H., Morsut, L., Liu, Z., Brar, G.A., Torres, S.E., Stern-Ginossar, N., Brandman, O., Whitehead, E.H., Doudna, J.A., et al. (2013). CRISPR-mediated modular RNA-guided regulation of transcription in eukaryotes. Cell *154*, 442–451.

Gossen, M., and Bujard, H. (1992). Tight control of gene expression in mammalian cells by tetracycline-responsive promoters. Proc. Natl. Acad. Sci. USA *89*, 5547–5551.

Greber, D., El-Baba, M.D., and Fussenegger, M. (2008). Intronically encoded siRNAs improve dynamic range of mammalian gene regulation systems and toggle switch. Nucleic Acids Res. *36*, e101.

Haurwitz, R.E., Sternberg, S.H., and Doudna, J.A. (2012). Csy4 relies on an unusual catalytic dyad to position and cleave CRISPR RNA. EMBO J. *31*, 2824–2832.

Hooshangi, S., Thiberge, S., and Weiss, R. (2005). Ultrasensitivity and noise propagation in a synthetic transcriptional cascade. Proc. Natl. Acad. Sci. USA *102*, 3581–3586.

Jiang, W., Bikard, D., Cox, D., Zhang, F., and Marraffini, L.A. (2013). RNA-guided editing of bacterial genomes using CRISPR-Cas systems. Nat. Biotechnol. *31*, 233–239.

Jinek, M., Chylinski, K., Fonfara, I., Hauer, M., Doudna, J.A., and Charpentier, E. (2012). A programmable dual-RNA-guided DNA endonuclease in adaptive bacterial immunity. Science *337*, 816–821.

Jinek, M., East, A., Cheng, A., Lin, S., Ma, E., and Doudna, J. (2013). RNA-programmed genome editing in human cells. eLife *2*, e00471.

Kalderon, D., Roberts, B.L., Richardson, W.D., and Smith, A.E. (1984). A short amino acid sequence able to specify nuclear location. Cell *39*, 499–509.

Karlsson, M., Weber, W., and Fussenegger, M. (2012). Design and construction of synthetic gene networks in mammalian cells. Methods Mol. Biol. *813*, 359–376.

Khalil, A.S., Lu, T.K., Bashor, C.J., Ramirez, C.L., Pyenson, N.C., Joung, J.K., and Collins, J.J. (2012). A synthetic biology framework for programming eukaryotic transcription functions. Cell *150*, 647–658.

Lin, R., Maeda, S., Liu, C., Karin, M., and Edgington, T.S. (2007). A large noncoding RNA is a marker for murine hepatocellular carcinomas and a spectrum of human carcinomas. Oncogene *26*, 851–858.

Maeder, M.L., Linder, S.J., Cascio, V.M., Fu, Y., Ho, Q.H., and Joung, J.K. (2013). CRISPR RNA-guided activation of endogenous human genes. Nat. Methods *10*, 977–979.

Mali, P., Aach, J., Stranges, P.B., Esvelt, K.M., Moosburner, M., Kosuri, S., Yang, L., and Church, G.M. (2013a). CAS9 transcriptional activators for target specificity screening and paired nickases for cooperative genome engineering. Nat. Biotechnol. *31*, 833–838.

Mali, P., Yang, L., Esvelt, K.M., Aach, J., Guell, M., DiCarlo, J.E., Norville, J.E., and Church, G.M. (2013b). RNA-guided human genome engineering via Cas9. Science *339*, 823–826.

Mercer, T.R., Dinger, M.E., and Mattick, J.S. (2009). Long non-coding RNAs: insights into functions. Nat. Rev. Genet. *10*, 155–159.

Milyavsky, M., Tabach, Y., Shats, I., Erez, N., Cohen, Y., Tang, X., Kalis, M., Kogan, I., Buganim, Y., Goldfinger, N., et al. (2005). Transcriptional programs following genetic alterations in p53, INK4A, and H-Ras genes along defined stages of malignant transformation. Cancer Res. *65*, 4530–4543.

Nissim, L., and Bar-Ziv, R.H. (2010). A tunable dual-promoter integrator for targeting of cancer cells. Mol. Syst. Biol. *6*, 444.

Nissim, L., Beatus, T., and Bar-Ziv, R. (2007). An autonomous system for identifying and governing a cell's state in yeast. Phys. Biol. *4*, 154–163.

Orioli, A., Pascali, C., Pagano, A., Teichmann, M., and Dieci, G. (2012). RNA polymerase III transcription control elements: themes and variations. Gene *493*, 185–194.

Perez-Pinera, P., Kocak, D.D., Vockley, C.M., Adler, A.F., Kabadi, A.M., Polstein, L.R., Thakore, P.I., Glass, K.A., Ousterout, D.G., Leong, K.W., et al. (2013). RNA-guided gene activation by CRISPR-Cas9-based transcription factors. Nat. Methods *10*, 973–976.

Pley, H.W., Flaherty, K.M., and McKay, D.B. (1994). Three-dimensional structure of a hammerhead ribozyme. Nature *372*, 68–74.

Proudfoot, N.J. (2011). Ending the message: poly(A) signals then and now. Genes Dev. *25*, 1770–1782.

Purcell, O., Peccoud, J., and Lu, T.K. (2013). Rule-Based Design of Synthetic Transcription Factors in Eukaryotes. ACS Synth. Biol. http://dx.doi.org/10.1021/sb400134k.

Qi, L., Haurwitz, R.E., Shao, W., Doudna, J.A., and Arkin, A.P. (2012). RNA processing enables predictable programming of gene expression. Nat. Biotechnol. *30*, 1002–1006.

Reyon, D., Tsai, S.Q., Khayter, C., Foden, J.A., Sander, J.D., and Joung, J.K. (2012). FLASH assembly of TALENs for high-throughput genome editing. Nat. Biotechnol. *30*, 460–465.

Rogakou, E.P., Pilch, D.R., Orr, A.H., Ivanova, V.S., and Bonner, W.M. (1998). DNA double-stranded breaks induce histone H2AX phosphorylation on serine 139. J. Biol. Chem. *273*, 5858–5868.

Saito, H., Kobayashi, T., Hara, T., Fujita, Y., Hayashi, K., Furushima, R., and Inoue, T. (2010). Synthetic translational regulation by an L7Ae-kink-turn RNP switch. Nat. Chem. Biol. *6*, 71–78.

Sander, J.D., and Joung, J.K. (2014). CRISPR-Cas systems for editing, regulating and targeting genomes. Nat. Biotechnol. *32*, 347–355, http://dx.doi.org/10.1038/nbt.2842.

Shin, K.J., Wall, E.A., Zavzavadjian, J.R., Santat, L.A., Liu, J., Hwang, J.I., Rebres, R., Roach, T., Seaman, W., Simon, M.I., and Fraser, I.D. (2006). A single lentiviral vector platform for microRNA-based conditional RNA interference and coordinated transgene expression. Proc. Natl. Acad. Sci. USA *103*, 13759–13764.

Sinha, A., Hughes, K.R., Modrzynska, K.K., Otto, T.D., Pfander, C., Dickens, N.J., Religa, A.A., Bushell, E., Graham, A.L., Cameron, R., et al. (2014). A cascade of DNA-binding proteins for sexual commitment and development in Plasmodium. Nature *507*, 253–257.

Smith, C.W.J., Porro, E.B., Patton, J.G., and Nadal-Ginard, B. (1989). Scanning from an independently specified branch point defines the 3′ splice site of mammalian introns. Nature *342*, 243–247.

Soukup, G.A., and Breaker, R.R. (1999). Design of allosteric hammerhead ribozymes activated by ligand-induced structure stabilization. Structure *7*, 783–791.

Sternberg, S.H., Haurwitz, R.E., and Doudna, J.A. (2012). Mechanism of substrate selection by a highly specific CRISPR endoribonuclease. RNA *18*, 661–672.

Stewart, S.A., Dykxhoorn, D.M., Palliser, D., Mizuno, H., Yu, E.Y., An, D.S., Sabatini, D.M., Chen, I.S., Hahn, W.C., Sharp, P.A., et al. (2003). Lentivirus-delivered stable gene silencing by RNAi in primary cells. RNA *9*, 493–501.

Taggart, A.J., DeSimone, A.M., Shih, J.S., Filloux, M.E., and Fairbrother, W.G. (2012). Large-scale mapping of branchpoints in human pre-mRNA transcripts in vivo. Nat. Struct. Mol. Biol. *19*, 719–721.

Upadhyay, S.K., Kumar, J., Alok, A., and Tuli, R. (2013). RNA-Guided Genome Editing for Target Gene Mutations in Wheat. G3 (Bethesda) *3*, 2233–2238.

Urlinger, S., Baron, U., Thellmann, M., Hasan, M.T., Bujard, H., and Hillen, W. (2000). Exploring the sequence space for tetracycline-dependent transcriptional activators: novel mutations yield expanded range and sensitivity. Proc. Natl. Acad. Sci. USA *97*, 7963–7968.

Wang, D., Wang, H., Brown, J., Daikoku, T., Ning, W., Shi, Q., Richmond, A., Strieter, R., Dey, S.K., and DuBois, R.N. (2006). CXCL1 induced by prostaglandin E2 promotes angiogenesis in colorectal cancer. J. Exp. Med. *203*, 941–951.

Weber, W., and Fussenegger, M. (2012). Emerging biomedical applications of synthetic biology. Nat. Rev. Genet. *13*, 21–35.

Wilson, R.C., and Doudna, J.A. (2013). Molecular mechanisms of RNA interference. Annu. Rev. Biophys *42*, 217–239.

Wilusz, J.E., JnBaptiste, C.K., Lu, L.Y., Kuhn, C.D., Joshua-Tor, L., and Sharp, P.A. (2012). A triple helix stabilizes the 3′ ends of long noncoding RNAs that lack poly(A) tails. Genes Dev. *26*, 2392–2407.

Xie, Z., Wroblewska, L., Prochazka, L., Weiss, R., and Benenson, Y. (2011). Multi-input RNAi-based logic circuit for identification of specific cancer cells. Science *333*, 1307–1311.

Ye, H., Daoud-El Baba, M., Peng, R.W., and Fussenegger, M. (2011). A synthetic optogenetic transcription device enhances blood-glucose homeostasis in mice. Science *332*, 1565–1568.

Yin, Q.-F., Yang, L., Zhang, Y., Xiang, J.-F., Wu, Y.-W., Carmichael, G.G., and Chen, L.-L. (2012). Long noncoding RNAs with snoRNA ends. Mol. Cell *48*, 219–230.

Molecular Cell, Volume *54*

Supplemental Information

Multiplexed and Programmable Regulation of Gene Networks with an Integrated RNA and CRISPR/Cas Toolkit in Human Cells

Lior Nissim, Samuel D. Perli, Alexandra Fridkin, Pablo Perez-Pinera, and Timothy K. Lu

Supplemental Data

Figure S1

A. Triplex/Csy4 gRNA expression mechanism

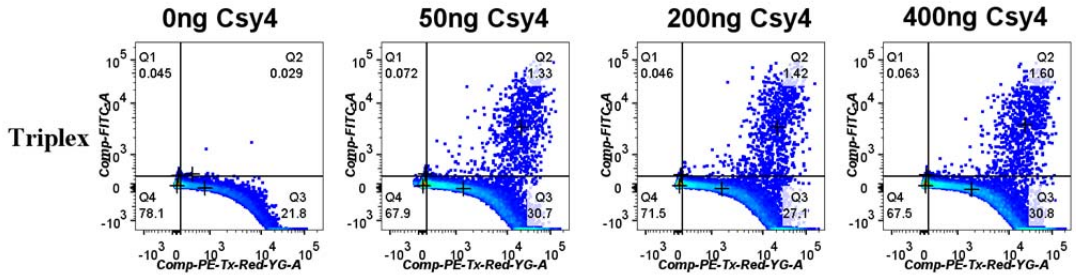

B. Intron/Csy4 gRNA expression mechanism

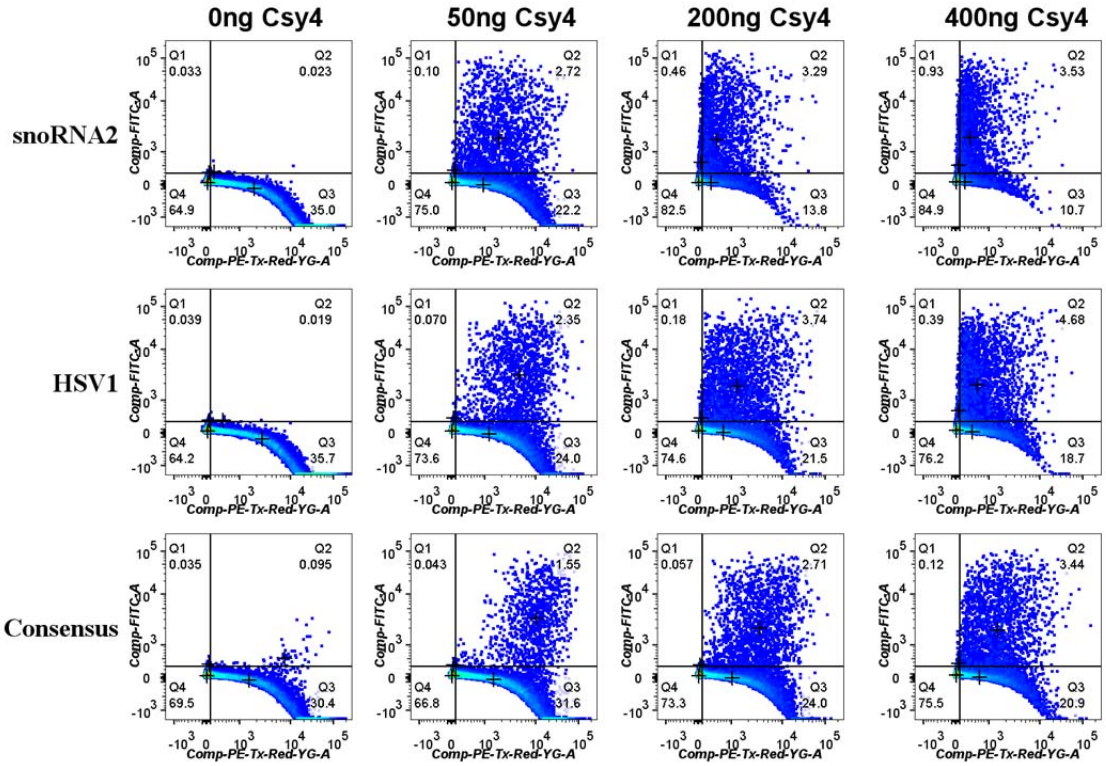

Figure S1. Flow cytometry data corresponding to: **(A)** the 'triplex/Csy4' strategy (Figure 1) and **(B)** the 'intron/Csy4' (Figure 2) strategy for generating functional gRNAs from RNAP II transcripts.

Abbreviations: *Comp-PE-Tx-Red-YG-A* (mKate2); *Comp-FITC-A* (EYFP).

Triplex: construct #3 (CMVp-*mK*-Tr-28-g1-28, 1 µg).

HSV1, consensus, and snoRNA2: constructs #4, 8, and 9, respectively (CMVp-mK_{EX1}-[28-g1-28]$_{\text{'intron type'}}$-mK_{EX2} with the corresponding intron sequences flanking the gRNA and Csy4 recognition sites ('28')). These plasmids were transfected at 1 µg.

In addition, the amount of the Csy4-expressing plasmid (construct #2) transfected in each sample is indicated. Other plasmids transfected included construct #1 (taCas9, 1 µg) and #5 (P1-*EYFP*, 1 µg).

Figure S2

A. Triplex/Csy4 mechanism with Cas9 and/or Csy4 controls

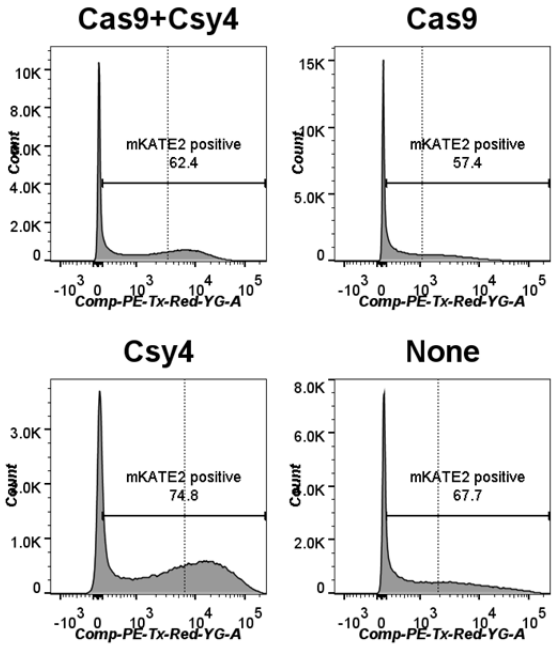

B. Additional controls for the Triplex/Csy4 and Intron/Csy4 mechanisms

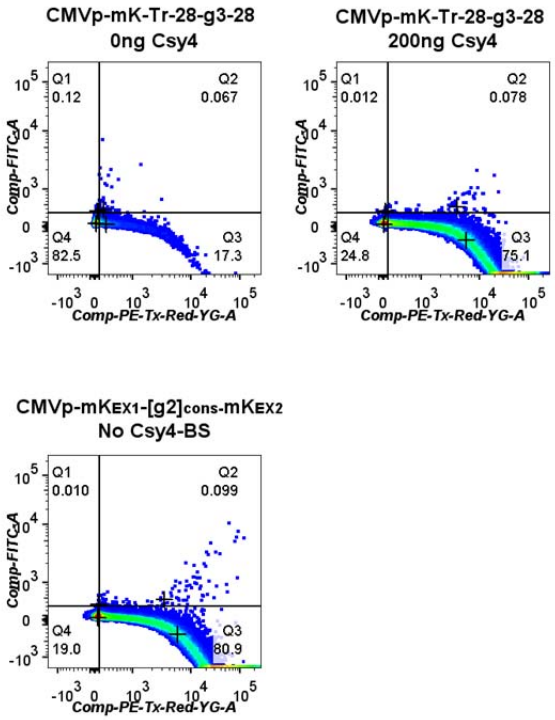

C. Guide RNA crosstalk controls

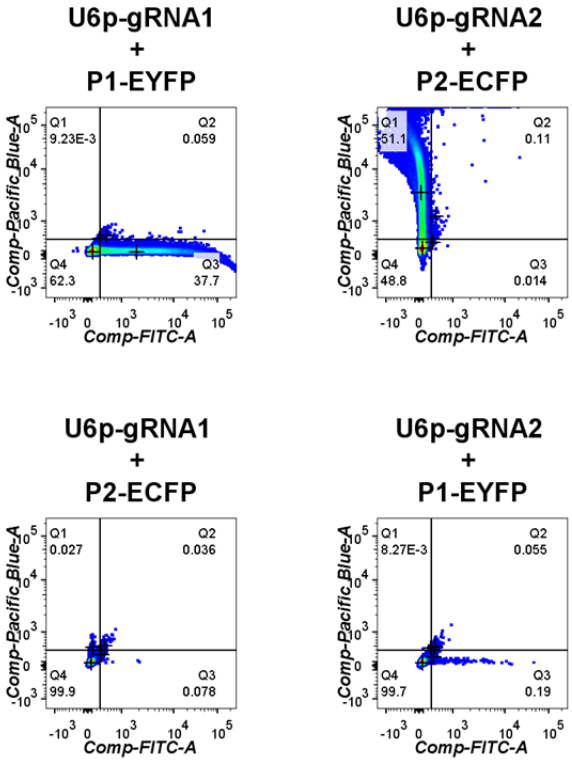

Figure S2. (A) Flow cytometry data corresponding to Figure 1C to analyze how various combinations of Csy4 and taCas9 affect expression of the harboring *mKate2* gene for the CMVp-*mK*-Tr-28-g1-28 architecture. All samples contained construct #3 (CMVp-*mK*-Tr-28-g1-28, 1 µg). Construct #1 (taCas9, 1 µg) and construct #2 (Csy4, 100 ng) were applied as indicated.

(B) Flow cytometry data providing various controls to demonstrate minimal non-specific activation of the P1 promoter by gRNA3 (top two panels). The amount of Csy4 DNA transfected in each sample in the top two panels is indicated. Other plasmids transfected in this experiment included construct #1 (taCas9, 1 µg) and construct #5 (P1-*EYFP*, 1 µg).

Flow cytometry data providing a control to demonstrate minimal EYFP activation from the promoter P2 with intronic gRNA2 without Csy4 binding sites (bottom panel). The lower panel (CMVp-mK_{EX1}-$[g2]_{cons}$-mK_{EX2}, construct #12) was tested in the absence of Csy4. Other plasmids transfected in this experiment included construct #1 (taCas9, 1 µg) and construct #27 (P2-*EYFP*, 1 µg).

(C) Flow cytometry data corresponding to controls made to validate that no crosstalk exists between gRNA1 and promoter P2 or between gRNA2 and promoter P1. All samples were transfected with the constructs listed in each plot title (1 µg each).

Abbreviations: *Comp-PE-Tx-Red-YG-A* (mKate2)*; Comp-FITC-A* (EYFP); *Comp-Pacific Blue-A* (ECFP).

Figure S3
Exploring the effects of Csy4 recognition site configurations flanking a gRNA

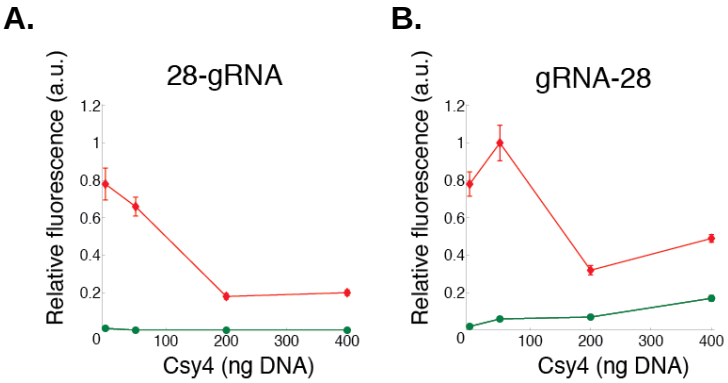

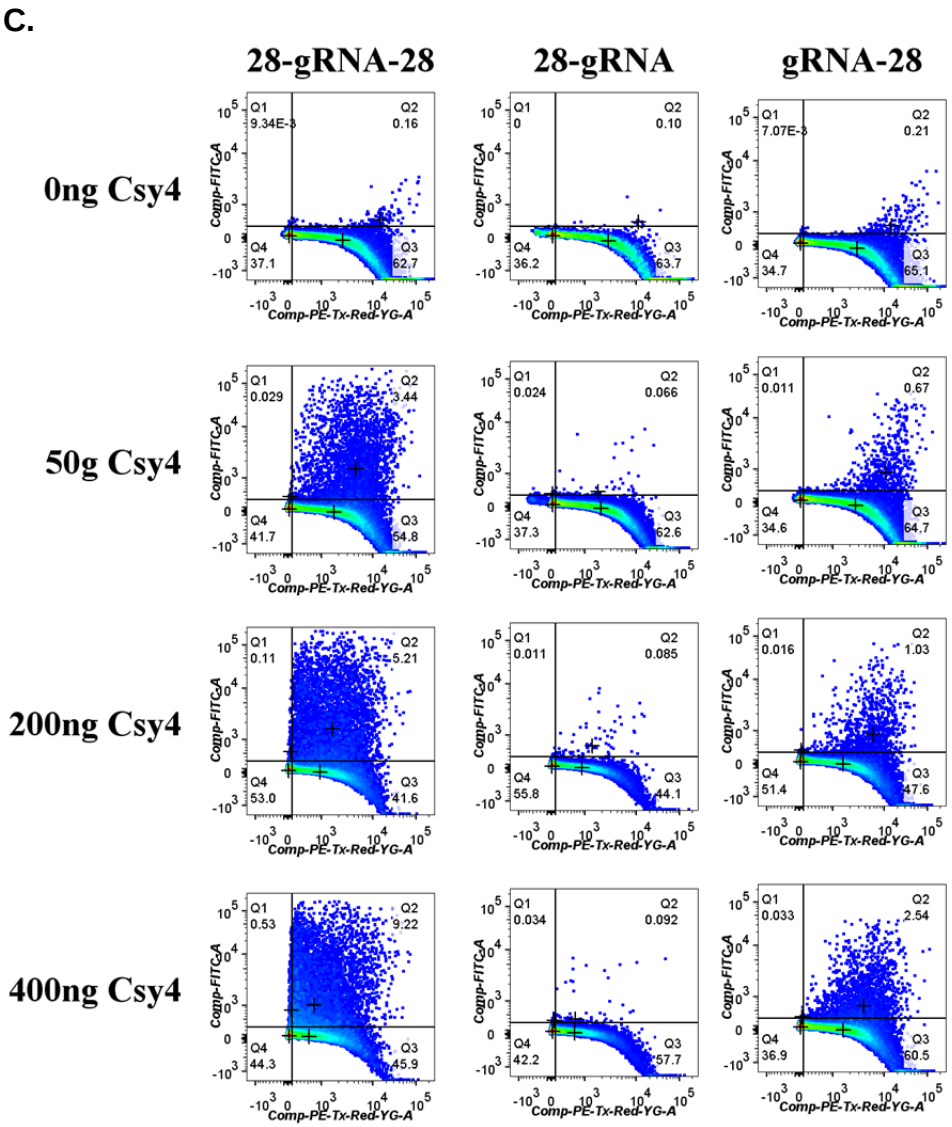

Figure S3. To determine whether both of the 5' and 3' Csy4 recognition sites are necessary for functional gRNA generation from introns, we tested a few variants of the HSV1-based intron within *mKate2* (Figure 2A). This intron housed a gRNA1 sequence that was either preceded by a Csy4 binding site on its 5' side ('28-gRNA', Figure S3A) or was followed by a Csy4 binding site on its 3' end ('gRNA-28', Figure S3B). The synthetic P1-*EYFP* construct was used to assess gRNA1 activity. The data for Figure S3A-B was normalized with the performance of the 'intron/Csy4' architecture where the intronic gRNA1 was flanked by two Csy4 binding sites ('28-gRNA-28') (Figure S3C). Data are represented as mean +/- SEM. Red lines and data points correspond to mKate fluorescence while green lines and data points correspond to EYFP fluorescence.

The single-Csy4-binding-site architectures had mKate2 levels that decreased with the addition of Csy4 (Figure S3A-B). The downstream *EYFP* activation by the gRNA1-directed CRISPR-TF was significantly lower for the single Csy4-binding-site architectures (Figure S3A-B) versus the 'intron/Csy4' construct (Figure 2D and Figure S3C). When only one Csy4 binding site was located at the 5' end of the gRNA1 intron, *EYFP* expression was nearly undetectable (Figure S3A). When only one Csy4 binding site was located at the 3' end of the gRNA1 intron, a 6-fold reduction in EYFP levels was observed (Figure S3B) compared with the 'intron/Cys4' architecture that contains two Csy4 recognition sites flanking gRNA1 (Figure 2D and Figure S3C).

These results demonstrate that while the 5' Csy4 recognition sequence is important for generating functional intronic gRNAs, the 3' Csy4 binding site is essential. We hypothesize that Csy4 can help stabilize intronic gRNA through several potential mechanisms. The 5' end of RNAs cleaved by Csy4 contain a hydroxyl (OH^-) which may protect them from major 5'→3' cellular RNases such as the XRN family, which require a 5' phosphate for substrate recognition (Houseley and Tollervey, 2009; Nagarajan et al., 2013). In addition, binding of the Csy4 protein to the 3' end of the cleaved gRNA (Haurwitz et al., 2012) may protect it from 3'→5' degradation mediated by the eukaryotic exosome complex (Houseley and Tollervey, 2009).

Figure S3C shows the flow cytometry data for analyzing how the various configurations of Csy4 recognition sites flanking the gRNA within the HSV1 intron affect CRISPR-TF activity. The fluorescence values for Figure S3A and S3B were normalized to the maximum fluorescence levels between these experiments and the $[28\text{-}g1\text{-}28]_{HSV1}$ control (Figure S3C).

Abbreviations: *Comp-PE-Tx-Red-YG-A* (mKate2); *Comp-FITC-A* (EYFP).

'28-gRNA-28' is HSV1 intronic gRNA flanked by two Csy4 recognition sites (construct #4, CMVp-mK_{EX1}-$[28\text{-}g1\text{-}28]_{HSV1}$-$mK_{EX2}$)
'28-gRNA' is HSV1 intronic gRNA with a 5' Csy4 recognition site only (construct #10, CMVp-mK_{EX1}-$[28\text{-}g1]_{HSV1}$-mK_{EX2})
'gRNA-28' is HSV1 intronic gRNA with a 3' Csy4 recognition site only (construct #11, CMVp-mK_{EX1}-$[g1\text{-}28]_{HSV1}$-mK_{EX2}).

In addition, the amount of the Csy4-expressing plasmid transfected in each sample is indicated with each figure. Other plasmids transfected in this experiment include construct #1 (taCas9, 1 µg) and construct #5 (P1-*EYFP*, 1 µg).

Figure S4
Engineering ribozymes to release functional gRNAs from RNAP II transcripts

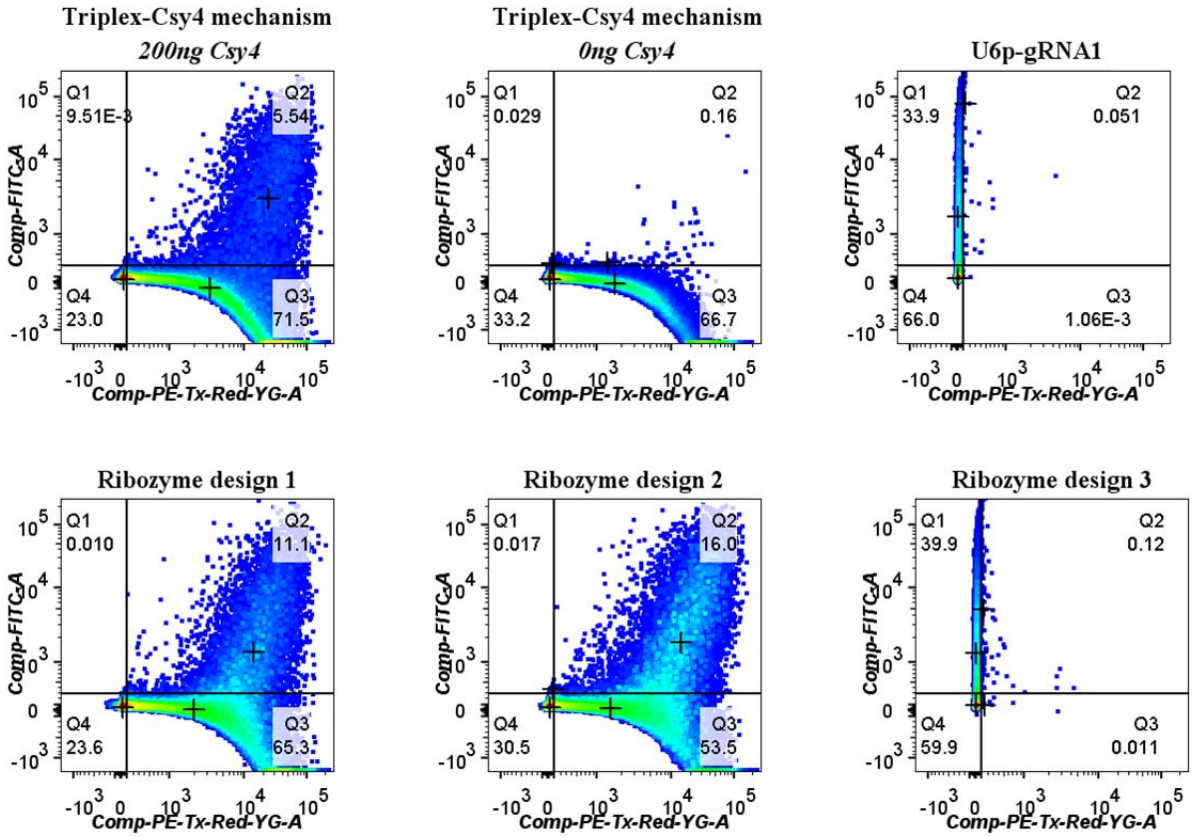

Figure S4. Flow cytometry data corresponding to Figure 3.

Abbreviations: *Comp-PE-Tx-Red-YG-A* (mKate2); *Comp-FITC-A* (EYFP).

'Triplex-Csy4' mechanism contains construct #3 (CMVp-*mK*-Tr-28-g1-28). Other plasmids transfected in this experiment include construct #1 (taCas9, 1 µg); construct #5 (P1-*EYFP*, 1 µg); construct #2 (Csy4, concentrations indicated).

'Ribozyme design 1' contains construct #13 (CMVp-*mK*-Tr-HH-g1-HDV). Other plasmids transfected in this experiment include construct #1 (taCas9, 1 µg); construct #5 (P1-*EYFP*, 1 µg).

'Ribozyme design 2' contains construct #14 (CMVp-*mK*-HH-g1-HDV). Other plasmids transfected in this experiment include construct #1 (taCas9, 1 µg); construct #5 (P1-*EYFP*, 1 µg).

'Ribozyme design 3' contains construct #15 (CMVp-HH-g1-HDV). Other plasmids transfected in this experiment include construct #1 (taCas9, 1 µg); construct #5 (P1-*EYFP*, 1 µg).

'U6p-gRNA1' contains construct #7 (U6p-g1, 1 µg). Other plasmids transfected in this experiment include construct #1 (taCas9, 1 µg) and construct #5 (P1-*EYFP*, 1 µg)

Figure S5
Multiplexed expression of 2x gRNAs from a single transcript

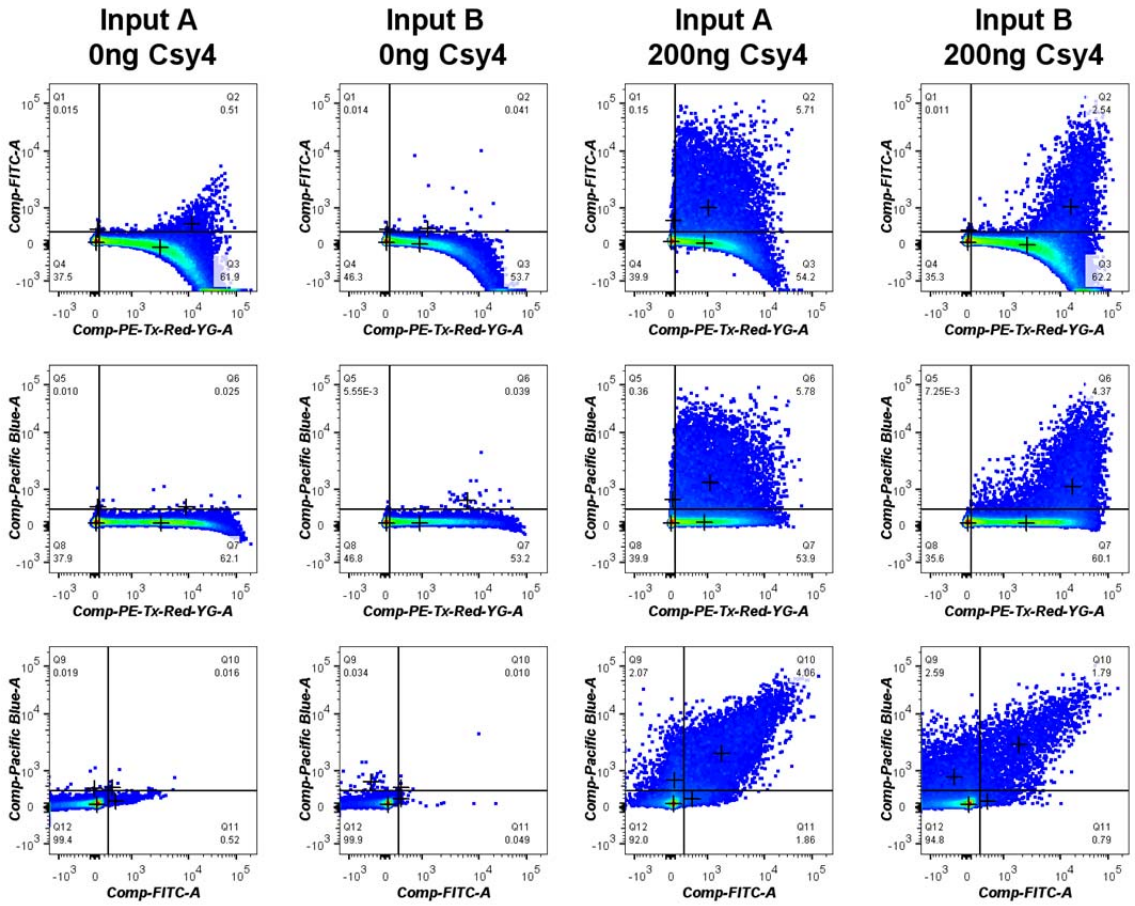

Figure S5. Flow cytometry data corresponding to Figure 4.

Abbreviations: *Comp-PE-Tx-Red-YG-A* (mKate2); *Comp-FITC-A* (EYFP); *Comp-Pacific Blue-A* (ECFP).

'Input A' refers to the 'intron-triplex' architecture and contains constructs #16 (CMVp-mK_{EX1}-[28-g1-28]$_{HSV1}$-mK_{EX2}-Tr-28-g2-28, 1 µg); #5 (P1-*EYFP*, 1 µg); #6 (P2-*ECFP*, 1 µg); and #1 (taCas9, 1 µg), as shown in Figure 4A.

'Input B' refers to the 'triplex-tandem' architecture and contains constructs #17 (CMVp-*mK*-Tr-28-g1-28-g2-28, 1 µg); #5 (P1-*EYFP*, 1 µg) and #6 (P2-*ECFP*, 1 µg); and #1 (taCas9, 1 µg), as shown in Figure 4B.

In addition, the amount of Csy4-producing plasmid DNA (construct #2) transfected in each sample is indicated above each plot.

Figure S6
Synthetic transcriptional cascades

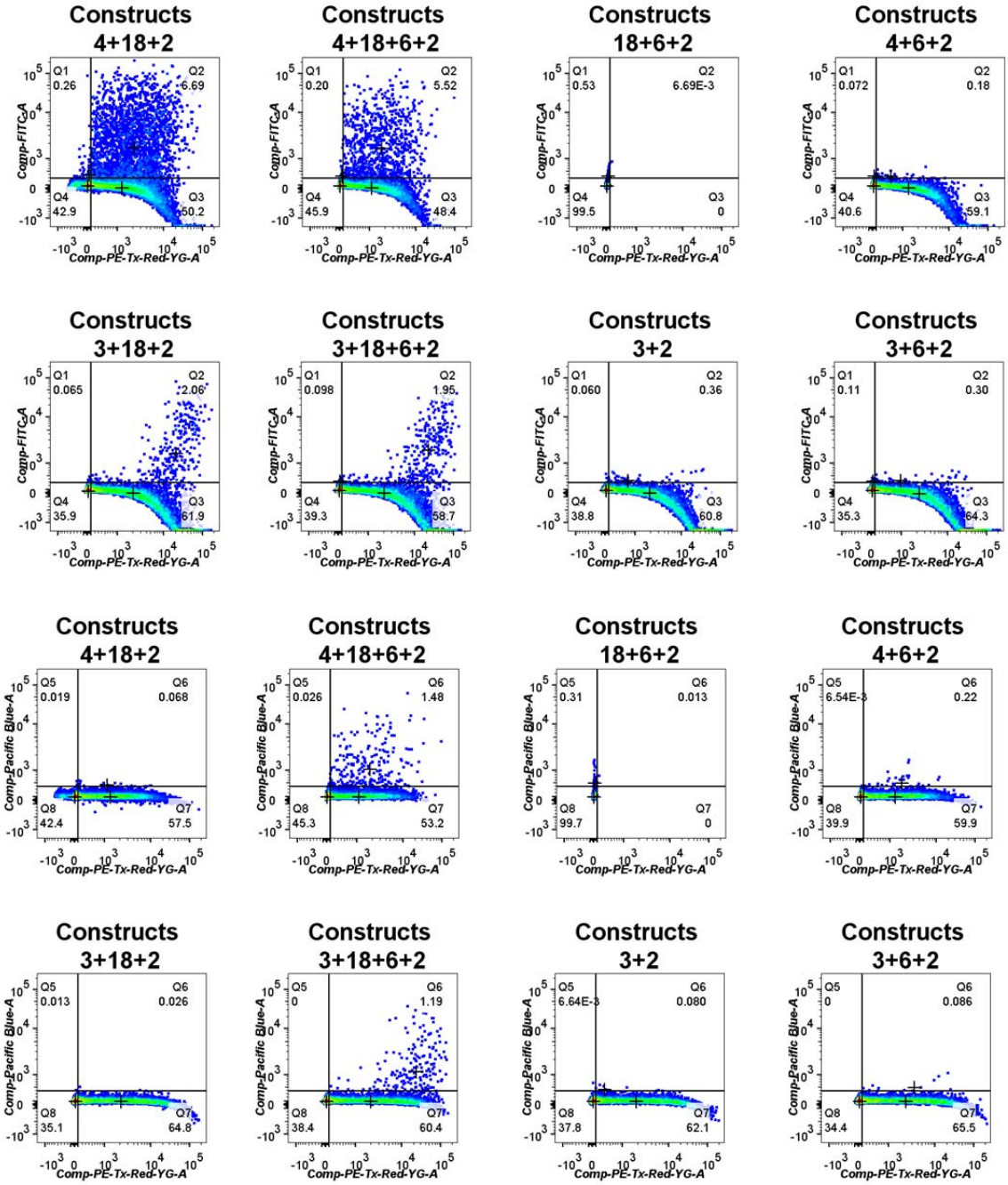

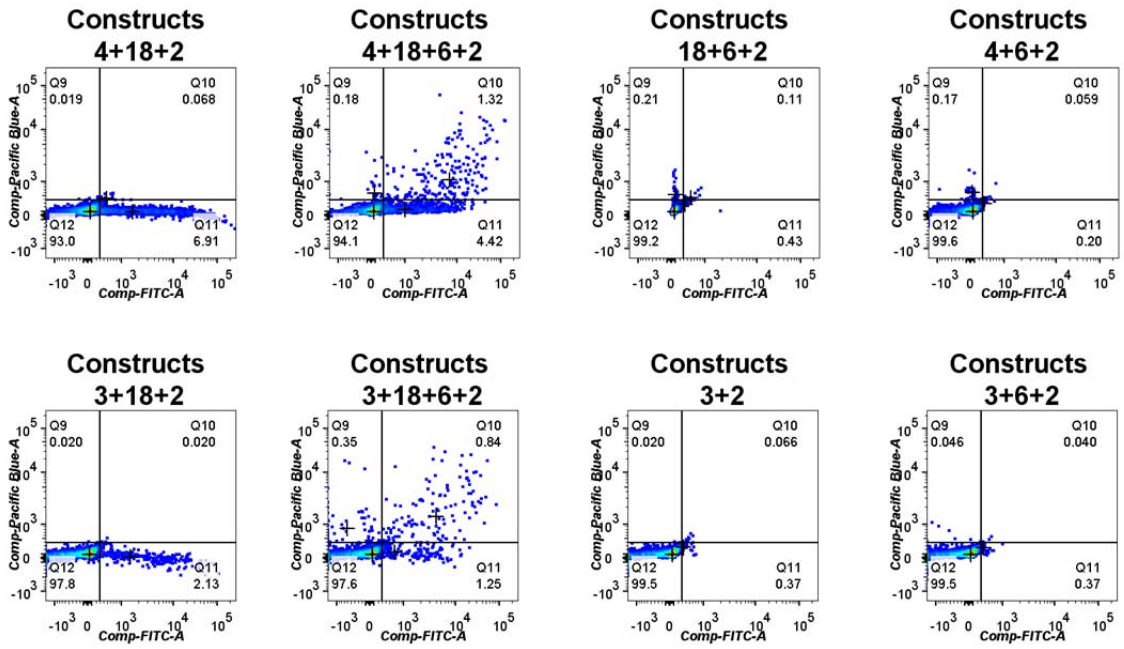

Figure S6. Flow cytometry data corresponding to Figure 6.

Abbreviations: *Comp-PE-Tx-Red-YG-A* (mKate2); *Comp-FITC-A* (EYFP); *Comp-Pacific Blue-A* (ECFP).

All samples were transfected with the constructs listed in each plot title (1 µg each, Table S1) as well as construct #1 (taCas9, 1 µg).

Figure S7
Rewiring synthetic circuit interconnections with Csy4

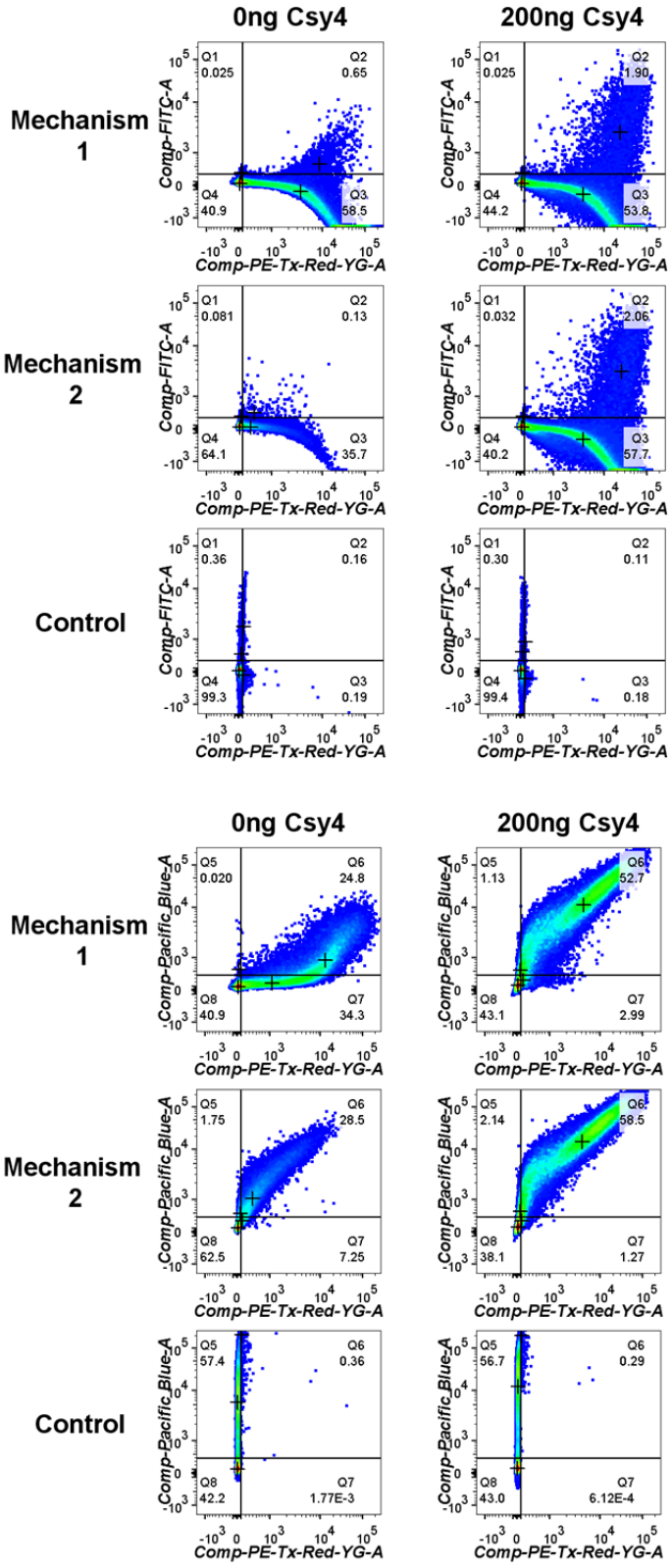

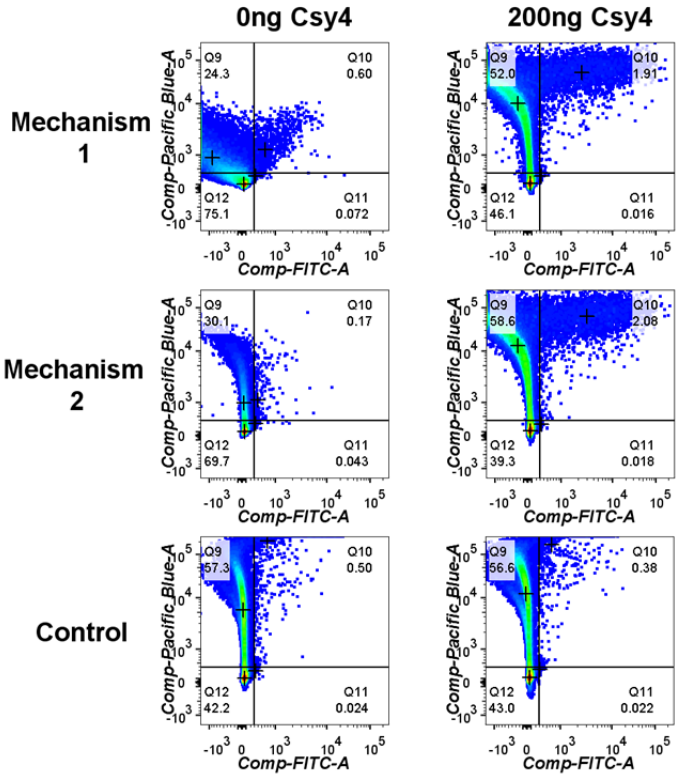

Figure S7. Flow cytometry data corresponding to Figure 7.

Abbreviations: *Comp-PE-Tx-Red-YG-A* (mKate2); *Comp-FITC-A* (EYFP); *Comp-Pacific Blue-A* (ECFP).

'Mechanism 1' contains the following constructs: #20 (CMVp-*mK*$_{EX1}$-[miR]-*mK*$_{EX2}$-Tr-28-g1-28); #22 (CMVp-*ECFP*-Tr-28-miR$_{8xBS}$-28); and #5 (P1-*EYFP*). These plasmids were transfected at a concentration of 1 µg each. This mechanism corresponds to the circuit diagram in Figure 7A.

'Mechanism 2' contains the following constructs: #21 (CMVp-*mK*$_{EX1}$-[miR]-*mK*$_{EX2}$-Tr-28-g1-28-miR$_{4xBS}$); #22 (CMVp-*ECFP*-Tr-28-miR$_{8xBS}$-28); and #5 (P1-*EYFP*). These plasmids were transfected at a concentration of 1 µg each. This mechanism corresponds to the circuit diagram in Figure 7D.

'Control' samples contain constructs #22 (CMVp-*ECFP*-Tr-28-miR$_{8xBS}$-28) and #5 (P1-*EYFP*) only. These plasmids were transfected at a concentration of 1 µg each.

In addition, the amount of Csy4-expressing plasmid (construct #2) transfected in each sample is indicated above each plot.

Table S1. Construct names, designs, and abbreviations

Construct 1	**CMVp-*dCas9-3xNLS-VP64*-3'LTR**
Abbreviation	taCas9
Construct 2	**PGK1p-*Csy4*-pA**
Abbreviation	Csy4
Construct 3	**CMVp-*mKate2*-Triplex-28-gRNA1-28-pA**
Abbreviation	CMVp-*mK*-Tr-28-g1-28
Construct 4	**CMVp-*mKate2*_EX1-[28-gRNA1-28]$_{HSV1}$-*mKate2*_EX2-pA**
Abbreviation	CMVp-*mK*$_{EX1}$-[28-g1-28]$_{HSV1}$-*mK*$_{EX2}$
Construct 5	**P1-*EYFP*-pA**
Abbreviation	P1-*EYFP*
Construct 6	**P2-*ECFP*-pA**
Abbreviation	P2-*ECFP*
Construct 7	**U6p-gRNA1-TTTTT**
Abbreviation	U6p-g1
Construct 8	**CMVp-*mKate2*_EX1-[28-gRNA1-28]$_{consensus}$-*mKate2*_EX2-pA**
Abbreviation	CMVp-*mK*$_{EX1}$-[28-g1-28]$_{cons}$-*mK*$_{EX2}$
Construct 9	**CMVp-*mKate2*_EX1-[28-gRNA1-28]$_{snoRNA2}$-*mKate2*_EX2-pA**
Abbreviation	CMVp-*mK*$_{EX1}$-[28-g1-28]$_{sno}$-*mK*$_{EX2}$
Construct 10	**CMVp-*mKate2*_EX1-[28-gRNA1]$_{HSV1}$-*mKate2*_EX2-pA**
Abbreviation	CMVp-*mK*$_{EX1}$-[28-g1]$_{HSV1}$-*mK*$_{EX2}$
Construct 11	**CMVp-*mKate2*_EX1-[gRNA1-28]$_{HSV1}$-*mKate2*_EX2-pA**
Abbreviation	CMVp-*mK*$_{EX1}$-[g1-28]$_{HSV1}$-*mK*$_{EX2}$
Construct 12	**CMVp-*mKate2*_EX1-[gRNA2]$_{consensus}$-*mKate2*_EX2-pA**
Abbreviation	CMVp-*mK*$_{EX1}$-[g2]$_{cons}$-*mK*$_{EX2}$
Construct 13	**CMVp-*mKate2*-Triplex-HHRibo-gRNA1-HDVRibo-pA**
Abbreviation	CMVp-*mK*-Tr-HH-g1-HDV
Construct 14	**CMVp-*mKate2*-HHRibo-gRNA1-HDVRibo-pA**
Abbreviation	CMVp-*mK*-HH-g1-HDV
Construct 15	**CMVp-HHRibo-gRNA1-HDVRibo-pA**

Abbreviation	CMVp-HH-g1-HDV
Construct 16	**CMVp-*mKate2*_EX1-[28-gRNA1-28]$_{HSV1}$-*mKate2*_EX2-Triplex-28-gRNA2-28-pA**
Abbreviation	CMVp-*mK*$_{EX1}$-[28-g1-28]$_{HSV1}$-*mK*$_{EX2}$-Tr-28-g2-28
Construct 17	**CMVp-*mKate2*-Triplex-28-gRNA1-28-gRNA2-28-pA**
Abbreviation	CMVp-*mK*-Tr-28-g1-28-g2-28
Construct 18	**P1-*EYFP*-Triplex-28-gRNA2-28-pA**
Abbreviation	P1-*EYFP*-Tr-28-g2-28
Construct 19	**CMVp-*mKate2*-Triplex-28-gRNA3-28-gRNA4-28-gRNA5-28-gRNA6-28**
Abbreviation	CMVp-*mK*-Tr-(28-g-28)$_{3-6}$
Construct 20	**CMVp-*mKate2*_EX1-[miRNA]-*mKate2*_EX2-Triplex-28-gRNA1-28-pA**
Abbreviation	CMVp-*mK*$_{EX1}$-[miR]-*mK*$_{EX2}$-Tr-28-g1-28
Construct 21	**CMVp-*mKate2*_EX1-[miRNA]-*mKate2*_EX2-Triplex-28-gRNA1-28-4xmiRNA-BS-pA**
Abbreviation	CMVp-*mK*$_{EX1}$-[miR]-*mK*$_{EX2}$-Tr-28-g1-28-miR$_{4xBS}$
Construct 22	**CMVp-*ECFP*-Triplex-28-8xmiRNA-BS-28-pA**
Abbreviation	CMVp-*ECFP*-Tr-28-miR$_{8xBS}$-28
Construct 23	**CMVp-*mKate2*-Triplex-28-gRNA3-28**
Abbreviation	CMVp-*mK*-Tr-28-g3-28
Construct 24	**CMVp-*mKate2*-Triplex-28-gRNA4-28**
Abbreviation	CMVp-*mK*-Tr-28-g4-28
Construct 25	**CMVp-*mKate2*-Triplex-28-gRNA5-28**
Abbreviation	CMVp-*mK*-Tr-28-g5-28
Construct 26	**CMVp-*mKate2*-Triplex-28-gRNA6-28**
Abbreviation	CMVp-*mK*-Tr-28-g6-28
Construct 27	**P2-*EYFP*-pA**
Abbreviation	P2-*EYFP*

Extended Experimental Procedures

Compensation controls

Compensation controls were strict and designed to remove false-positive cells even at the cost of removing true-positive cells. Compensation was done with BD FACSDiva (version no. 6.1.3; BD Biosciences) as detailed below:

Table S3. Compensation setup for flow cytometry

Fluorochrome	-% Fluorochrome	Spectral Overlap
PE-Tx-Red-YG	FITC	0%
Pacific Blue	FITC	0.2%
FITC	PE-Tx-Red-YG	21.1%
Pacific Blue	PE-Tx-Red-YG	1%
FITC	Pacific Blue	7.5%

Flow cytometry analysis

Compensated flow cytometry results were analyzed using FlowJo software (vX.0.7r2). Calculations were performed as described below:

1. All samples were gated to exclude cell clumps and debris (population P1)

2. Histograms of P1 cells were analyzed according to the following gates, which were determined according to the auto-fluorescence of non-transfected cells in the same acquisition conditions such that the proportion of false-positive cells would be lower than 0.1%:
    a. mKate2: ‘mKate2 positive’ cells were defined as cells above a fluorescence threshold of 100 a.u.
    b. EYFP: ‘EYFP positive’ cells were defined as cells above a fluorescence threshold of 300 a.u.
    c. ECFP: ‘ECFP positive’ cells were defined as cells above a fluorescence threshold of 400 a.u.

3. The percent of positive cells (% positive) and the median fluorescence for each ‘positive cell’ population were calculated. The % positive cells was multiplied by the median fluorescence, resulting in a weighted median fluorescence expression level that correlated fluorescence intensity with cell numbers. This measurement strategy is consistent with several previous studies (Auslander et al., 2012; Xie et al., 2011).

4. The weighted median fluorescence was determined for each sample. The mean of the weighted median fluorescence of biological triplicates was calculated. These are the data presented in the paper. The standard error of the mean (SEM) was also computed and presented as error bars.

5. To facilitate comparisons between various constructs and to account for variations in the brightness of different fluorescent proteins, the weighted median fluorescence for each experimental condition was divided by the maximum weighted median fluorescence for the same fluorophore among all conditions tested in the same set of experiments.

Flow cytometry data plots shown in the Supplemental Information are representative compensated data from a single experiment. As noted above, cells were gated to exclude cell clumps and debris (population P1), and the entire gated population of viable cells are presented in each figure. The threshold for each sub-population Q1-Q4 was set according to the thresholds described above. The percentage of cells in each sub-population is indicated in the plots. Black crosses in the plots indicate the median fluorescence for a specific sub-population.

Plasmid construction

The plasmid **CMVp-*mKate2*-Triplex-28-gRNA1-28-pA** (Construct 3, Table S1) was built using Gibson Assembly from three parts amplified with appropriate homology overhangs: 1) the full length coding sequence of *mKate2*; 2) the first 110 bp of the mouse MALAT1 3' triple helix (Wilusz et al., 2012); and 3) gRNA1 containing a 20 bp Specificity Determining Sequence (SDS) and a *S. pyogenes* gRNA scaffold along with 28nt Csy4 recognition sites.

The reporter plasmids **P1-*EFYP*-pA** (Construct 5, Table S1), **P2-*ECFP*-pA** (Construct 6, Table S1) and **P2-*EYFP*-pA** (Construct 27, Table S1) were built by cloning in repeated gRNA1 binding sites and repeated gRNA2 binding sites into the NheI site of **pG5-Luc** (Promega) via annealing complementary oligonucleotides. Then, *EYFP* and *ECFP* were cloned into the NcoI/FseI sites, respectively.

The plasmid **CMVp-*mKate2*_EX1-[28-gRNA1-28]$_{HSV1}$-*mKate2*_EX2-pA** (Construct 4, Table S1) was built by Gibson Assembly of the following parts with appropriate homology overhangs: 1) the *mKate2*_EX1 (a.a. 1-90) of *mKate2*; 2) *mKate*_EX2 (a.a. 91-237) of *mKate2*; and 3) gRNA1 containing a 20bp SDS followed by the *S. pyogenes*

gRNA scaffold flanked by Csy4 recognition sites and the HSV1 acceptor, donor and branching sequences. Variations of the **CMVp-*mKate2*_EX1-[28-gRNA1-28]$_{HSV1}$-*mKate2*_EX2-pA** plasmid containing consensus and snoRNA2 acceptor, donor, and branching sequences and with and without the Csy4 recognition sequences (Constructs 8-11, Table S1) were built in a similar fashion.

The ribozyme-expressing plasmids **CMVp-*mKate2*-Triplex-HHRibo-gRNA1-HDVRibo-pA** and **CMVp-*mKate2*-HHRibo-gRNA1-HDVRibo-pA** plasmids (Constructs 13 and 14, respectively, Table S1) were built by Gibson Assembly of XmaI-digested **CMVp-*mKate2***, and PCR-extended amplicons of gRNA1 (with and without the triplex and containing HHRibo (Gao and Zhao, 2014) on the 5' end and HDVRibo (Gao and Zhao, 2014) on the 3' end). The plasmid **CMVp-HHRibo-gRNA1-HDVRibo-pA** (Construct 15, Table S1) was built similarly by Gibson Assembly of SacI-digested **CMVp-*mKate2*** and a PCR-extended amplicon of gRNA1 containing HHRibo on the 5' end and HDVRibo on the 3' end.

The plasmid **CMVp-*mKate2*_EX1-[28-gRNA1-28]$_{HSV1}$-*mKate2*_EX2-Triplex-28-gRNA2-28-pA** (Construct 16, Table S1) was built by Gibson Assembly of the following parts using appropriate homologies: 1) XmaI-digested **CMVp-*mKate2*_EX1-[28-gRNA1-28]$_{HSV1}$-*mKate2*_EX2-pA** (Construct 4, Table S1) and 2) PCR amplified Triplex-28-gRNA2-28 from **CMVp-*mKate2*-Triplex-28-gRNA1-28-pA** (Construct 3, Table S1).

The plasmid **CMVp-*mKate2*-Triplex-28-gRNA1-28-gRNA2-28-pA** (Construct 17, Table S1) was built by Gibson Assembly with the following parts using appropriate homologies: 1) XmaI-digested **CMVp-*mKate2*-Triplex-28-gRNA1-28-pA** (Construct 3, Table S1) and 2) PCR amplified 28-gRNA2-28.

The plasmid **CMVp-*mKate2*-Triplex-28-gRNA3-28-gRNA4-28-gRNA5-28-gRNA6-28** (Construct 19, Table S1) was constructed using a Golden Gate approach using the Type IIs restriction enzyme, BsaI (Engler and Marillonnet, 2013), as shown below:

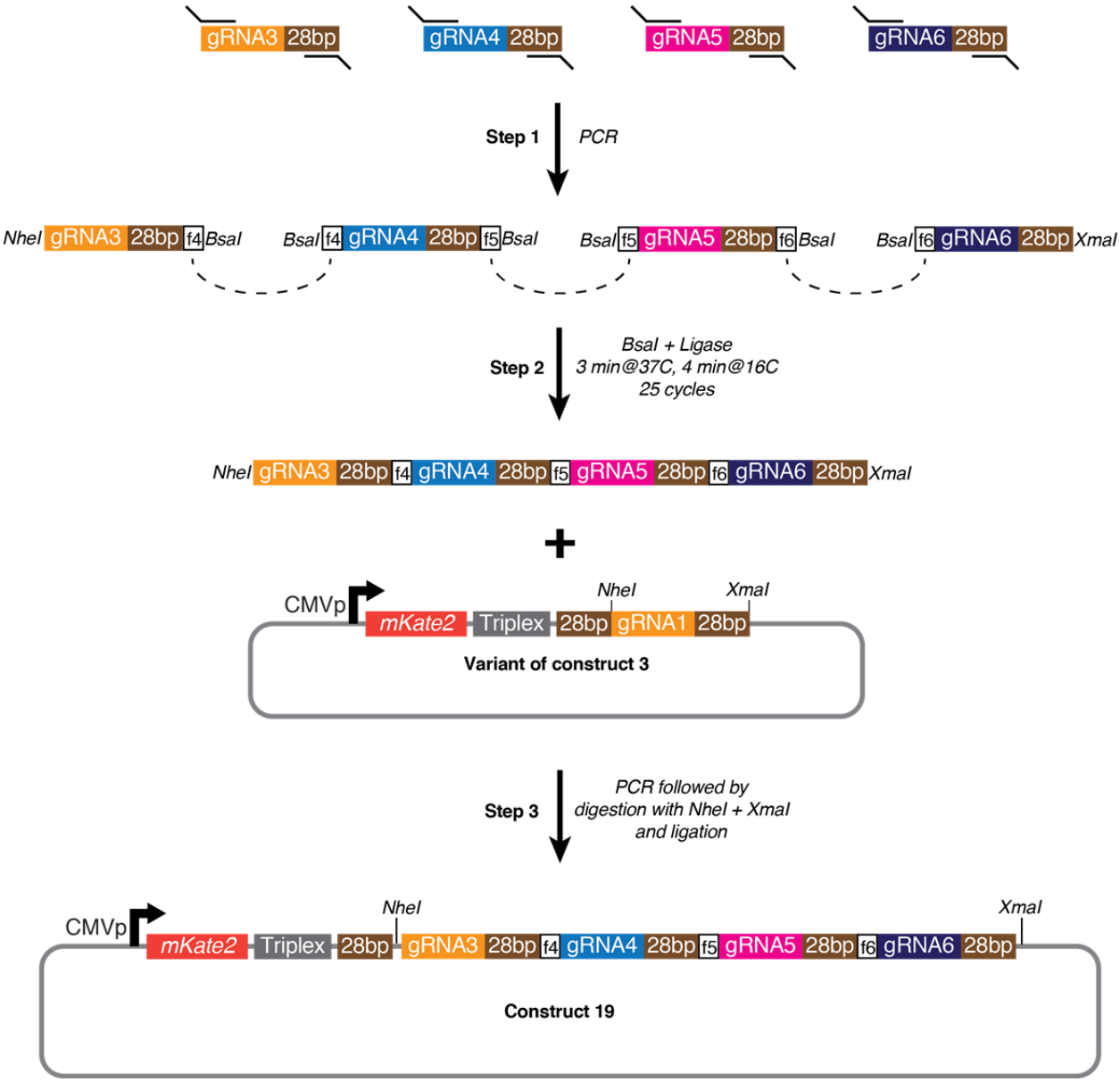

Step 1 – Each individual gRNA of interest (e.g., gRNA3, gRNA4, etc.) containing a 20 bp SDS followed by the *S. pyogenes* gRNA scaffold and a Csy4 '28' sequence was PCR amplified to be flanked on both the 5' and 3' ends by the BsaI type IIs restriction enzyme site. Short, 5 base pair sequences (e.g., f3, f4, etc.) were introduced on the 5' and 3' ends immediately downstream and upstream of the BsaI sites, respectively. These 5 bp sequences were designed

such that each adjoining gRNA to be cloned would contain the same 5 bp sequence.

Step 2 – The amplified products containing the BsaI sites were mixed in a single reaction mixture containing the enzyme BsaI and T4 DNA ligase. The reaction mixture was subjected to 25 repeats of 3 minute digestions followed by 4 minute ligations at 37°C and 16°C, respectively.

Step 3 – The assembled product containing all the gRNAs of interest from Step 2 was further PCR amplified to produce a larger amount of the assembled gRNA construct. This product was then digested with NheI-HF and XmaI and cloned into the **CMVp-*mKate2*-Triplex-28-gRNA1-28** plasmid (a variant of Construct 3, Table S1).

The CMVp-*mKate2*_EX1-[miRNA]-*mKate2*_EX2-pA plasmid containing an intronic FF4 (a synthetic miRNA) was received as a gift from Lila Wroblewska. The synthetic FF4 miRNA was cloned into an intron with consensus acceptor, donor and branching sequences between a.a. 90 and 91 of mKate2 to create **CMVp-*mKate2*_EX1-[miRNA]-*mKate2*_EX2-Triplex-28-gRNA1-28-pA** (Construct 20, Table S1) and **CMVp-*mKate2*_EX1-[miRNA]-*mKate2*_EX2-Triplex-28-gRNA1-28-4xmiRNA-BS-pA** (Construct 21, Table S1).

The plasmid **CMVp-*ECFP*-Triplex-28-8xmiRNA-BS-28-pA** (Construct 22, Table S1) was cloned via Gibson Assembly with the following parts: 1) full length coding sequence of ECFP and 2) 110 nt of the MALAT1 3' triple helix sequence amplified via PCR extension with oligonucleotides containing eight FF4 miRNA binding sites and Csy4 recognition sequences on both ends. Cloning protocol for multiplexed gRNA expression constructs

Quantitative reverse transcription–PCR (RT-PCR)

The experimental procedure followed was as described in (Perez-Pinera et al., 2013). Cells were harvested 72h post-transfection. Total RNA was isolated by using the RNeasy Plus RNA isolation kit (Qiagen). cDNA synthesis was performed by using qScript cDNA SuperMix (Quanta Biosciences). Real-time PCR using PerfeCTa SYBR Green FastMix (Quanta Biosciences) was performed with the Mastercycler ep realplex real-time PCR system (Eppendorf) with oligonucleotide primers, which were as follows:

IL1RN: forward GGAATCCATGGAGGGAAGAT
reverse TGTTCTCGCTCAGGTCAGTG

GAPDH: forward CAATGACCCCTTCATTGACC
reverse TTGATTTTGGAGGGATCTCG

The primers were designed using Primer3Plus software and purchased from IDT. Melting curve analysis was used to confirm primer specificity. To ensure linearity of the standard curve, reaction efficiencies over the appropriate dynamic range were calculated. Using the ddCt method, we calculated fold-increases in the mRNA expression of the gene of interest normalized to *GAPDH* expression. We then normalized the mRNA levels to the non-specific gRNA1 control condition. Reported values are the means of three independent biological replicates with technical duplicates that were averaged for each experiment. Error bars represent standard error of the mean (SEM).

Supplemental References

Auslander, S., Auslander, D., Muller, M., Wieland, M., and Fussenegger, M. (2012). Programmable single-cell mammalian biocomputers. Nature *487*, 123-127.

Engler, C., and Marillonnet, S. (2013). Combinatorial DNA assembly using Golden Gate cloning. Methods in molecular biology (Clifton, NJ) *1073*, 141-156.

Gao, Y., and Zhao, Y. (2014). Self-processing of ribozyme-flanked RNAs into guide RNAs in vitro and in vivo for CRISPR-mediated genome editing. Journal of Integrative Plant Biology, n/a-n/a.

Haurwitz, R.E., Sternberg, S.H., and Doudna, J.A. (2012). Csy4 relies on an unusual catalytic dyad to position and cleave CRISPR RNA. Embo j *31*, 2824-2832.

Houseley, J., and Tollervey, D. (2009). The Many Pathways of RNA Degradation. Cell *136*, 763-776.

Nagarajan, V.K., Jones, C.I., Newbury, S.F., and Green, P.J. (2013). XRN 5′->3′ exoribonucleases: Structure, mechanisms and functions. Biochimica et Biophysica Acta (BBA) - Gene Regulatory Mechanisms *1829*, 590-603.

Perez-Pinera, P., Kocak, D.D., Vockley, C.M., Adler, A.F., Kabadi, A.M., Polstein, L.R., Thakore, P.I., Glass, K.A., Ousterout, D.G., Leong, K.W.*, et al.* (2013). RNA-guided gene activation by CRISPR-Cas9-based transcription factors. Nat Meth *10*, 973-976.

Wilusz, J.E., JnBaptiste, C.K., Lu, L.Y., Kuhn, C.D., Joshua-Tor, L., and Sharp, P.A. (2012). A triple helix stabilizes the 3' ends of long noncoding RNAs that lack poly(A) tails. Genes & development *26*, 2392-2407.

Xie, Z., Wroblewska, L., Prochazka, L., Weiss, R., and Benenson, Y. (2011). Multi-Input RNAi-Based Logic Circuit for Identification of Specific Cancer Cells. Science *333*, 1307-1311.